Preparation and Molecular and Electronic Structures of Iron(0) Dinitrogen and Silane Complexes and Their Application to Catalytic Hydrogenation and Hydrosilation

Suzanne C. Bart, Emil Lobkovsky, and Paul J. Chirik*

Contribution from the Department of Chemistry and Chemical Biology, Baker Laboratory, Cornell University, Ithaca, New York 14853

Received June 2, 2004; E-mail: pc92@cornell.edu

Abstract: Reduction of the five-coordinate iron(II) dihalide complexes (^{iPr}PDI)FeX$_2$ (^{iPr}PDI = ((2,6-CHMe$_2$)$_2$C$_6$H$_3$N=CMe)$_2$C$_5$H$_3$N; X = Cl, Br) with sodium amalgam under 1 atm of dinitrogen afforded the square pyramidal, high spin iron(0) bis(dinitrogen) complex (^{iPr}PDI)Fe(N$_2$)$_2$. In solution, (^{iPr}PDI)Fe(N$_2$)$_2$ loses 1 equiv of N$_2$ to afford the mono(dinitrogen) adduct (^{iPr}PDI)Fe(N$_2$). Both dinitrogen compounds serve as effective precatalysts for the hydrogenation and hydrosilation of olefins and alkynes. Effecient catalytic reactions are observed with low catalyst loadings (≤0.3 mol %) at ambient temperature in nonpolar media. The catalytic hydrosilations are selective in forming the anti-Markovnikov product. Structural characterization of a high spin iron(0) alkyne and a bis(silane) σ-complex has also been accomplished and in combination with isotopic labeling studies provides insight into the mechanism of both catalytic C−H and catalytic C−Si bond formation.

Introduction

Catalytic bond forming reactions promoted by homogeneous transition metal complexes have become an indispensable tool in synthetic chemistry.[1] Most syntheses of complex molecular targets rely on one, if not many, key metal-mediated steps.[2] While unprecedented levels of activity and selectivity have been achieved,[3] increasing pressures for atom-economical[4] and catalytic processes with reduced environmental impact[5] fuel the search for improved synthetic transformations that minimize waste production, energy consumption, and generation of toxic substances.[6]

One approach to accomplishing this goal is to replace toxic, heavy metal catalysts with more benign iron compounds. For an effective process, however, the new catalysts should provide high activity at low loadings and high substrate concentrations ideally without organic solvent.[7,8] The low toxicity and high terrestrial abundance[9] of iron make it an attractive metal for this purpose. Work from several laboratories has recently focused on developing homogeneous iron catalysts as precious-metal surrogates.[10] Building on the seminal work of Kochi,[11] Fürstner[12−14] and Hayashi[15] have independently reported ef-

ficient C−C bond forming cross-coupling reactions, although in some cases the oxidation state and identity of the catalytically active iron species is not well understood. Iron catalysts have also been developed for olefin polymerization and display levels of activity and selectivity comparable to those of more traditional group 4 metallocene catalysts.[16,17]

These results suggested to us that iron, when in an appropriate coordination geometry and spin state, may be a reasonable alternative to precious metals in a wide range of catalytic bond forming reactions. Inspired by the success of iron catalysts in olefin polymerization[18] and reports on MAO-activated iron catalysts for olefin hydrogenation,[19,20] our initial focus was on reactions that involved insertion of an unsaturated organic molecule into an iron hydride or iron alkyl. Specifically, we

(1) Noyori, R. *Asymmetric Catalysis in Organic Synthesis*; Wiley: New York, 1994.
(2) Cornils, B.; Herrmann, W. A. *Applied Homogeneous Catalysis with Organometallic Compounds*; VCH: Weinheim, Germany, 1996.
(3) (a) Knowles, W. S. *Angew. Chem., Int. Ed.* **2002**, *41*, 1998. (b) Noyori, R. *Angew. Chem., Int. Ed.* **2002**, *41*, 2008. (c) Sharpless, K. B. *Angew. Chem., Int. Ed.* **2002**, *41*, 2024.
(4) Trost, B. M. *Acc. Chem. Res.* **2002**, *35*, 695.
(5) Baker, R. T.; Tumas, W. *Science* **1999**, *284*, 1477.
(6) Anastas, P. T.; Kirchhoff, M. M. *Acc. Chem. Res.* **2002**, *35*, 686.
(7) DeSimone, J. M. *Science* **2002**, *297*, 799.
(8) Hoge, G.; Wu, H.-P.; Kissel, W. S.; Pflum, D. A.; Greene, D. J.; Bao, J. *J. Am. Chem. Soc.* **2004**, *126*, 5966.
(9) Goldschmidt, V. W. *Geochemistry*; Oxford Press: London 1958; p 647.

(10) Examples of iron-catalyzed reactions: (a) tom Dieck, H.; Dietrich, J. *Chem. Ber.* **1984**, *117*, 694. (b) Corey, E. J.; Imai, N.; Zhang, H.-Y. *J. Am. Chem. Soc.* **1991**, *113*, 728. (c) Takacs, J. M.; Weidner, J. J.; Takacs, B. E. *Tetrahedron Lett.* **1993**, *34*, 6219. (d) Watahiki, T.; Akabane, Y.; Mori, S.; Oriyama, T. *Org. Lett.* **2003**, *5*, 3045.
(11) Kochi, J. K. *Acc. Chem. Res.* **1974**, *7*, 351.
(12) Fürstner, A.; Leitner, A.; Méndez, M.; Krause, H. *J. Am. Chem. Soc.* **2002**, *124*, 13856.
(13) Fürstner, A.; De Souza, D.; Parra-Rapado, L.; Jensen, J. T. *Angew. Chem., Int. Ed.* **2003**, *42*, 5358.
(14) (a) Siedel, G.; Laurich, D.; Fürstner, A. *J. Org. Chem.* **2004**, *69*, 3950. (b) Scheiper, B.; Bonnekessel, M.; Krause, H.; Fürstner, A. *J. Org. Chem.* **2004**, *69*, 3943.
(15) Nagano, T.; Hayashi, T. *Org. Lett.* **2004**, *6*, 1297.
(16) Small, B. L.; Brookhart, M.; Bennett, A. M. A. *J. Am. Chem. Soc.* **1998**, *120*, 4049.
(17) Britovsek, G. J. P.; Bruce, M.; Gibson, V. C.; Kimberley, B. S.; Maddox, P. J.; Mastroianni, S.; McTavish, S. J.; Redshaw, C.; Solan, G. A.; Strömberg, S.; White, A. J. P.; Williams, D. J. *J. Am. Chem. Soc.* **1999**, *121*, 8728.
(18) Bianchini, C.; Mantovani, G.; Meli, A.; Migliacci, F.; Zanobini, F.; Laschi, F.; Sommazzi, A. *Eur. J. Inorg. Chem.* **2003**, 1620.
(19) Knijnenburg, Q.; Horton, A. D.; Van Der Heijden, H.; Gal, A. W.; Budzelaar, P.; Henricus, M. PCT Int. Appl. WO 2003042131, 2003; 26 pp.
(20) Bart, S. C.; Chirik, P. J. Unpublished results.

are interested in developing highly active catalysts for both the hydrogenation and hydrosilation of unsaturated organic molecules, given the widespread synthetic utility of these reactions and their reliance on toxic, precious metals.[21−23]

We recently reported[24] the synthesis and characterization of a series of four-coordinate, and in some cases enantiopure, iron-(II) dialkyl complexes that are reluctant to participate in olefin and alkyne insertion reactions, possibly due to their high spin, $S = 2$ electronic configuration.[25] On the basis of these results, we began to explore alternative coordination geometries and spin states and were encouraged by the reports of 1-hexene hydrogenation by $Fe(CO)_5$.[26] However, the utility of these reactions is hampered by the high temperatures and pressures, typically in excess of 200 °C and 200−250 atm, required for catalytic activity. Likewise, Wrighton has developed a photocatalytic method for both olefin hydrogenation and hydrosilation using $Fe(CO)_5$ that operates efficiently at 22 °C and 1 atm of pressure, but continued irradiation with 366 nm light is required for turnover.[27] Bianchini and co-workers have reported a cationic iron hydride complex that hydrogenates alkynes to alkenes under mild conditions; however, further conversion of alkenes to alkanes is not observed.[28] Concurrent with our studies, Daida and Peters have developed a family of tris(phosphino)borato-ligated iron alkyl and hydride complexes that are competent for olefin and alkyne hydrogenation at room temperature and 1 atm of H_2.[29]

Here we describe the synthesis and characterization of an unusual high spin, d^8 square pyramidal iron(0) bis(dinitrogen) complex that serves as an effective precatalyst for the hydrogenation and selective hydrosilation of both olefins and alkynes. In addition, two catalytically competent intermediates, an iron alkyne compound and a bis(silane) σ-complex, have been synthesized and crystallographically characterized. These molecules, in combination with isotopic labeling studies, have provided insight into the mechanism of iron-catalyzed C−H and C−Si bond forming reactions.

Results and Discussion

Synthesis of the Well-Defined Catalyst Precursor 1-(N$_2$)$_2$. Inspired by Wrighton's findings that photogenerated $Fe(CO)_3$ is the active species in $Fe(CO)_5$-catalyzed olefin hydrogenation and isomerization reactions,[27] we targeted the synthesis of a well-defined iron precursor that could provide access to a reactive, 14-electron isolobal $L_3Fe(0)$ fragment under mild
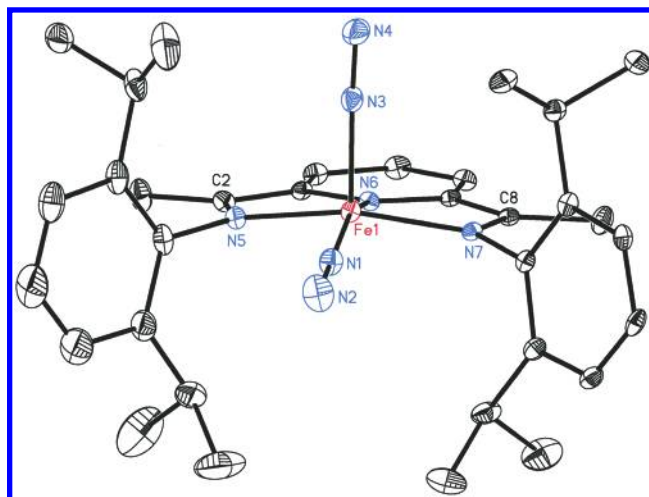
Figure 1. Molecular structure of **1-(N$_2$)$_2$** (30% probability ellipsoids). Hydrogen atoms omitted for clarity.

thermal conditions. Tridentate pyridinediimine (PDI) ligands of the general form $[(2,6-ArN=C(Me))_2C_5H_3N]$ (Ar = substituted aryl group) are attractive for this purpose given their relative ease of synthesis, modularity, and well-documented success in supporting catalytically active iron compounds.[16−19] In addition, the relative π-acidity of this class of molecule as compared to σ-donating trialkylphosphine ligands may also aid in stabilization of electron-rich Fe(0) complexes.

Reduction of the iron(II) dihalide complexes containing 2,6-diisopropylphenyl substituents, **1-Cl$_2$** or **1-Br$_2$**, with 0.5% sodium amalgam under 1 atm of dinitrogen produced green crystals identified as the five-coordinate iron(0) bis(dinitrogen) complex **1-(N$_2$)$_2$** (eq 1).
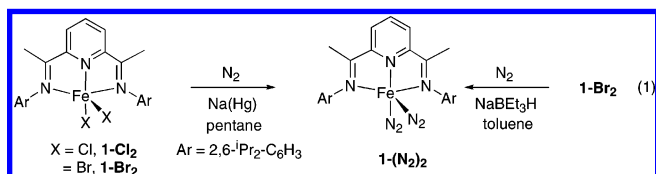
The bis(dinitrogen) compound can also be readily synthesized by addition of 2 equiv of $NaBEt_3H$ to **1-Br$_2$** in toluene. Presumably, generation of Fe(0) proceeds by facile reductive elimination of dihydrogen from the putative iron(II) dihydride **1-H$_2$**. Dark green **1-(N$_2$)$_2$** was characterized by a combination of IR and electronic spectroscopies, elemental analysis, and X-ray diffraction. Coordination of two N_2 ligands in the solid state was also confirmed by a Toepler pump experiment. Unlike ruthenium, where coordination of two N_2 ligands has been known for some time,[30,31] to our knowledge synthesis of **1-(N$_2$)$_2$** provides the first example of an iron(0) bis(dinitrogen) complex.

Single crystals of **1-(N$_2$)$_2$** suitable for X-ray diffraction were grown from a concentrated pentane/ether (∼10:1) solution. The solid-state structure is shown in Figure 1, and selected bond distances and angles are reported in Table 1. While several iron-(0) dinitrogen complexes have been reported,[32] only a limited number have been crystallographically characterized.[33] More

(21) Chaloner, P. A.; Esteruelas, M. A.; Joó, F.; Oro, L. A. *Homogeneous Hydrogenation*; Kluwer Academic Publishers: Dordrecht, The Netherlands, 1994.
(22) (a) Brook, M. A. *Silicon in Organic, Organometallic, and Polymer Chemistry*; Wiley: New York, 2000. (b) Ojima, I.; Li, Z.; Zhu, J. *The Chemistry of Organic Silicon Compounds*; Wiley: Avon, U.K., 1998; Chapter 29.
(23) Early-transition-metal and lanthanide catalysts are also effective for hydrogenation and hydrosilation. For representative examples see: (a) Troutman, M. V.; Apella, D. H.; Buchwald, S. L. *J. Am. Chem. Soc.* **1999**, *121*, 4916. (b) Conticello, V. P.; Brard, L.; Giardello, M. A.; Tsuji, Y.; Sabat, M.; Stern, C. L.; Marks, T. J. *J. Am. Chem. Soc.* **1992**, *114*, 2761. (c) Jeske, G.; Lauke, H.; Mauermann, H.; Schumann, H.; Marks, T. J. *J. Am. Chem. Soc.* **1985**, *107*, 8111.
(24) Bart, S. C.; Hawrelak, E. J.; Schmisseur, A. K.; Lobkovsky, E.; Chirik, P. J. *Organometallics* **2004**, *23*, 237.
(25) (a) Harvey, J. N.; Poli, R.; Smith, K. M. *Coord. Chem. Rev.* **2003**, *238*, 347−361. (b) Poli, R. *Chem. Rev.* **1996**, *96*, 2135.
(26) Harmon, R. E.; Gupta, S. K.; Brown, D. J. *Chem. Rev.* **1973**, *73*, 21.
(27) Schroeder, M. A.; Wrighton, M. S. *J. Am. Chem. Soc.* **1976**, *98*, 551.
(28) Bianchini, C.; Meli, A.; Peruzzini, M.; Frediani, P.; Bohanna, C.; Esteruelas, M. A.; Oro, L. A. *Organometallics* **1992**, *11*, 138.
(29) Daida, E. J.; Peters, J. C. *Inorg. Chem.* **2004**, in press.

(30) (a) Fergusson, J. E.; Love, J. L. *Chem. Commun.* **1969**, 399. (b) Kane-Maguire, L. A. P.; Sheridan, P. S.; Basolo, F.; Pearson, R. G. *J. Am. Chem. Soc.* **1968**, *90*, 5295.
(31) (a) Sellmann, D. *Angew. Chem., Int. Ed. Engl.* **1974**, *13*, 639. (b) Allen, A. D.; Harris, R. O.; Loescher, B. R.; Stevens, J. R.; Whiteley, R. N. *Chem. Rev.* **1973**, *73*, 11.

Table 1. Selected Bond Distances and Angles for **1-(N₂)₂**

	distance (Å)		angle (deg)
N(1)−N(2)	1.090(2)	Fe(1)−N(1)−N(2)	178.40(19)
N(3)−N(4)	1.104(3)	Fe(1)−N(3)−N(4)	171.81(17)
Fe(1)−N(1)	1.8341(16)	N(1)−Fe(1)−N(3)	98.02(8)
Fe(1)−N(3)	1.8800(19)	N(1)−Fe(1)−N(5)	96.65(7)
Fe(1)−N(6)	1.8362(14)	N(1)−Fe(1)−N(7)	97.41(7)
N(5)−C(2)	1.332(2)	N(5)−Fe(1)−N(6)	74.49(6)
N(7)−N(8)	1.333(2)	N(6)−Fe(1)−N(7)	79.90(6)
deviation of Fe(1)	0.297		
deviation of N(1)	0.072		

significantly, each of the previously structurally characterized iron(0) dinitrogen complexes contains only one N_2 ligand and adopts a trigonal bipyramidal geometry.

The molecular geometry about the iron in **1-(N₂)₂** is best described as a distorted square pyramid with one N_2 ligand completing the fourth site of the basal plane while the other occupies the apical position. The basal N_2 ligand lies 0.072 Å below the plane defined by N(5)−N(6)−N(7) of the PDI ligand. In contrast, the iron atom deviates more significantly, lying 0.297 Å above the plane defined by N(5)−N(6)−N(7). As with other structurally characterized iron complexes containing the ^{iPr}PDI ligand,[16−18] the aryl substituents are oriented perpendicular to the basal plane of the molecule. The geometric preference for square pyramidal over pseudo trigonal bipyramidal is most likely steric in origin. Several (PDI)Fe^{II} complexes that adopt a trigonal bipyramidal geometry have been reported,[18] but those that incorporate the bulky 2,6-diisopropyl ligand seem to favor square pyramidal coordination.[16] In this present case, placing two dinitrogen ligands axially would produce unfavorable steric interactions with the aryl substituents perpendicular to the plane of the PDI ligand.

Both the bond distances and vibrational stretching frequencies of the N_2 ligands are consistent with minimal activation by the d^8 iron center. The basal and apical N_2 ligands have N−N bond distances of 1.090(2) and 1.104(3) Å, respectively, and are indistinguishable from each other and free N_2 according to the 3σ criterion. Curiously, the apical N_2 ligand is significantly bent with an Fe(1)−N(3)−N(4) angle equal to 171.81(17)°. For comparison, the basal N_2 ligand is more linear with an Fe(1)−N(1)−N(2) angle of 178.40(19)°. The observed N−N bond distances are in good agreement with the N−N bond distance of 1.142(7) Å reported for (depe)₂Fe(N₂) (depe = diethylphosphinoethane)[33b] and the value of 1.078(30) Å found in (Et₃P)₂(CO)₂Fe(N₂).[33a]

The absence of significant π-back-bonding is further corroborated by the observation of two strong N−N stretches centered at 2053 and 2124 cm^{-1} in the solid-state (KBr pellet) infrared spectrum. Most iron(0) dinitrogen complexes supported by phosphine ligands have N_2 stretching frequencies between 1950 and 2068 cm^{-1}.[32,33] The higher frequencies observed for **1-(N₂)₂** are consistent with the π-accepting nature of the PDI ligand relative to the phosphines and make the observed N_2 stretching frequencies intermediate to the value of 2098 cm^{-1} reported for (PEt₃)₂(CO)₂Fe(N₂)[33a] and the range of 2060−2130 cm^{-1} typically found in iron(II) dinitrogen complexes.[34]

The solid-state magnetic susceptibility of **1-(N₂)₂** was investigated by SQUID magnetometry (see the Supporting Information). Variable temperature data collected from 4 to 300 K are consistent with a paramagnetic molecule that has an excellent fit ($R^2 = 0.995$) to the Curie−Weiss law. The observed values for the magnetic moment clearly establish an $S = 1$ ground state for **1-(N₂)₂**.

Five-coordinate, iron(0) complexes have been known for over a century, with Fe(CO)₅ being the most familiar example.[35] Since that time, several (CO)₄FeL and (CO)₃FeL₂ (L = phosphine) complexes have been prepared and a continuum of geometries[36,37] ranging between trigonal bipyramidal[38,39,40] and square pyramidal[41] have been observed. In addition, pentakis-(phosphine)iron(0) complexes have also been prepared and crystallographically characterized and both limiting geometries observed.[42,43] In many cases, attempts to measure the barrier to interconversion have been unsuccessful[44,45] owing to facile ligand site exchange by a classic Berry mechanism,[46] although a static A₂B₃-type spectrum has been observed for Fe(P(OMe)₃)₅ at −104 °C.[47] Importantly, each of the aforementioned complexes is *diamagnetic*, and thus, the triplet ground state observed for **1-(N₂)₂** is, to our knowledge, the first example of a high spin, d^8 iron(0) complex.[48] While unusual for iron, high spin, d^8 electronic configurations are well-known for isoelectronic Ni(II) complexes. Many of these molecules have been characterized by X-ray diffraction[49−51] and their electronic structures thoroughly investigated.[52] Formally, **1-(N₂)₂** can also be viewed as an intermediate spin iron(II) diamide complex where the PDI ligand has been reduced by a two-electron transfer from the iron center.

Attempts to characterize **1-(N₂)₂** in solution revealed interesting dynamic behavior. Dissolving the molecule in either pentane

(32) (a) George, T. A.; Rose, D. J.; Chang, Y.; Chen, Q.; Zubieta, J. *Inorg. Chem.* **1995**, *34*, 1295. (b) Cable, R. A.; Green, M.; Mackenzie, R. E.; Timms, P. L.; Turney, T. W. *Chem. Commun.* **1976**, 270. (c) Hills, A.; Hughes, D. L.; Jimenez-Tenorio, M.; Leigh, G. J.; Rowley, A. T. *J. Chem. Soc., Dalton Trans.* **1993**, 3041.
(33) (a) Kandler, H.; Gauss, C.; Bidell, W.; Rosenberger, S.; Burgi, T.; Eremenko, I. L.; Veghini, D.; Orama, O.; Burger, P.; Berke, H. *Chem.—Eur. J.* **1995**, *1*, 541. (b) Perhuisot, P.; Jones, W. D. *New J. Chem.* **1994**, *18*, 621. (c) Komiya, S.; Akita, M.; Yoza, A.; Kasuga, N.; Fukuoka, A.; Kai, Y. *Chem. Commun.* **1993**, 787. (d) Berke, H.; Bankhardt, W.; Huttner, G.; Vonseyrel, J.; Zsolnai, L. *Chem. Ber.* **1981**, *114*, 2754.

(34) Hirano, M.; Akita, M.; Morikita, T.; Kubo, H.; Fukuoka, A.; Komiya, S. *J. Chem. Soc., Dalton Trans.* **1997**, 3453.
(35) (a) Mond, L.; Quincke, F. *J. Chem. Soc.* **1891**, *59*, 604. (b) Berthelot, M. *C. R. Hebd. Seances Acad. Sci.* **1891**, *112*, 1343.
(36) Battaglia, L. P.; Delledonne, D.; Nardelli, M.; Pelizzi, C.; Predieri, G.; Chiusoli. G. P. *J. Organomet. Chem.* **1987**, *330*, 101.
(37) Cotton, F. A.; Hardcastle, K. I.; Rusholme, G. A. *J. Coord. Chem.* **1973**, *2*, 217.
(38) Cowley, A. H.; Davis, R. E.; Remadna, K. *Inorg. Chem.* **1981**, *20*, 2146.
(39) Allison, D. A.; Clardy, J.; Verkade, J. G. *Inorg. Chem.* **1972**, *11*, 2804.
(40) Howell, J. A. S.; Palin, M. G.; McArdle, P.; Cunningham, D.; Goldschmidt, Z.; Gottlieb, H. E.; Hezroni-Langerman, D. *Inorg. Chem.* **1993**, *32*, 3493.
(41) Casey, C. P.; Whiteker, G. T.; Campana, C. F.; Powell, D. R. *Inorg. Chem.* **1990**, *29*, 3376.
(42) Wong, W. K.; Chiu, K. W.; Wilkinson, G.; Howes, A. J.; Motevalli, M.; Hursthouse, M. B. *Polyhedron* **1985**, *4*, 603.
(43) Elschenbroich, C.; Nowotny, M.; Berhrendt, A.; Harms, K.; Wocadlo, S.; Pebler, J. *J. Am. Chem. Soc.* **1994**, *116*, 6217.
(44) Brookhart, M.; Chandler, W. A.; Pfister, A. C.; Santini, C. C.; White, P. S. *Organometallics* **1992**, *11*, 1263.
(45) Meakin, P.; Jesson, J. P. *J. Am. Chem. Soc.* **1973**, *95*, 7272.
(46) Meutterties, E. L. *Acc. Chem. Res.* **1970**, *3*, 266.
(47) Meakin, P.; English, A. D.; Ittel, S. D.; Jesson, J. P. *J. Am. Chem. Soc.* **1975**, *97*, 1254.
(48) Betley and Peters have recently reported an example of an $S = 1$, Fe(0) four-coordinate dinitrogen complex: Betley, T. A.; Peters, J. C. *J. Am. Chem. Soc.* **2003**, *125*, 10782.
(49) Sacconi, L.; Orioli, P. L.; DiVaira, M. *J. Am. Chem. Soc.* **1965**, *87*, 2059.
(50) Legg, J. I.; Nielson, D. O.; Smith, D. L.; Larson, M. L. *J. Am. Chem. Soc.* **1968**, *90*, 5030.
(51) Sacconi, L.; Mani, F.; Bencini, A. In *Comprehensive Coordination Chemistry*; Wilkinson, G., Gillard, R. D., McCleverty, J. A., Eds.; Pergamon: Oxford, 1987; Vol. 5.
(52) Furlani, C. *Coord. Chem. Rev.* **1968**, *3*, 141.
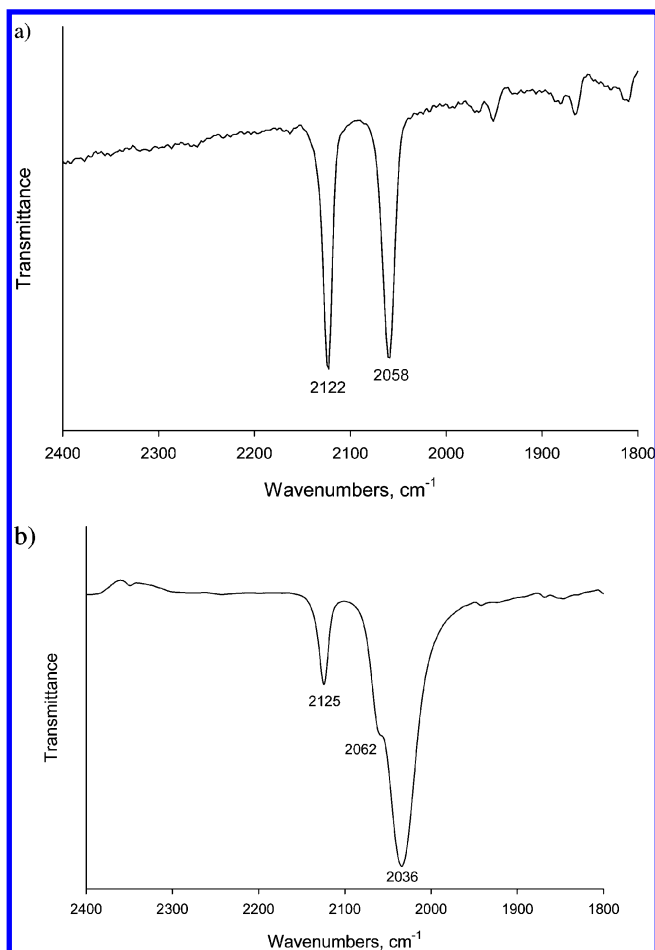
Figure 2. In situ React-IR data in toluene demonstrating reversible N_2 dissociation from **1-(N$_2$)$_2$**.

or toluene affords a dark, olive green solution. Monitoring the dissolution process with a Toepler pump experiment indicated loss of 1 equiv of dinitrogen, consistent with formation of **1-N$_2$** in solution (eq 2).
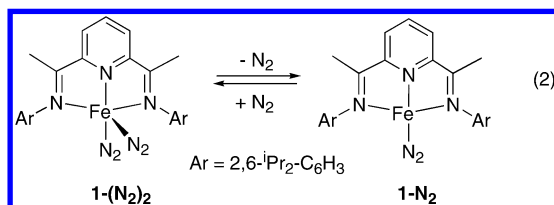

Further evidence for this equilibrium was also obtained by in situ infrared spectroscopy. In toluene at 23 °C, a single band centered at 2036 cm^{-1} is observed for **1-N$_2$** (Figure 2). Cooling the solution to −78 °C under an atmosphere of N_2 produces two additional bands centered at 2122 and 2058 cm^{-1}, in agreement with those observed for **1-(N$_2$)$_2$**. This behavior is reversible as repeated cooling and warming cycles produce the bands assigned to **1-(N$_2$)$_2$** and **1-N$_2$**, respectively. It should be noted that loss of N_2 from **1-(N$_2$)$_2$** is faster in toluene, perhaps owing to the greater solubility of dinitrogen in pentane.

The dynamic coordination and dissociation of dinitrogen from **1-(N$_2$)$_2$** was also investigated by NMR spectroscopy. At 25 °C, a solution magnetic moment of 2.52 μ_B was measured by Evans method[53] for **1-N$_2$** and is slightly lower than the value expected

for two unpaired electrons. The low magnetic moment may be due to spin−orbit coupling resulting in a quenching of the orbital angular moment as is typically encountered in square planar molecules.[54] Despite the $S = 1$ ground state, sharp, assignable ^{1}H NMR spectra are observed (Figure 3). These spectral features contrast those of related four-coordinate iron(II) complexes with $S = 2$ ground states where no H−H coupling is observed and the chemical shift dispersion is over 500 ppm.[16−18,24] The sharp resonances observed for samples of **1-N$_2$** prepared with rigorous exclusion of N_2 broaden upon exposure to dinitrogen, suggesting a dynamic equilibrium between the four- and five-coordinate compounds on the NMR time scale.

Synthesis and solid-state characterization of a high spin, d^8 square pyramidal iron(0) complex such as **1-(N$_2$)$_2$** suggests that addition of stronger field ligands may afford more familiar low spin, diamagnetic, iron(0) derivatives. Exposure of **1-(N$_2$)$_2$** to 1 atm of CO resulted in substitution of the dinitrogen ligands and produced the corresponding iron(0) dicarbonyl complex **1-(CO)$_2$** (eq 3).
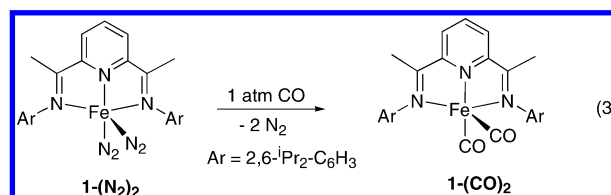
Olive green **1-(CO)$_2$** was characterized by a combination of elemental analysis and infrared, electronic, and multinuclear NMR spectroscopies. The pentane solution infrared spectrum of **1-(CO)$_2$** exhibits two strong CO bands centered at 1914 and 1974 cm^{-1}, demonstrating that, unlike **1-(N$_2$)$_2$**, both ligands are retained in solution. The infrared bands appear at lower frequency relative to the CO stretching frequencies of 2002 and 2024 cm^{-1} observed for neat Fe(CO)$_5$. This observation is consistent with the weaker field of the ^{iPr}PDI ligand relative to CO. As expected for a dynamic, five-coordinate Fe(0) complex, the ^{1}H and ^{13}C NMR spectra of **1-(CO)$_2$** recorded in benzene-d_6 or toluene-d_8 display the number of resonances expected for a molecule with C_{2v} symmetry. The origin of the ligand symmetrization is likely a Berry pseudorotation[46] where the apical and basal CO ligands are equivalent by a rocking through the plane of the iron.

Preparation of paramagnetic **1-(N$_2$)$_2$** and **1-N$_2$** along with a diamagnetic reference compound, **1-(CO)$_2$**, allows measurement of the magnitude of the isotropic chemical shifts of the mixture of dinitrogen compounds in solution. A detailed table of shifts and their temperature dependencies are presented in the Supporting Information. In general, the observed isotropic shifts are consistent with a spin delocalization mechanism where the hydrogens in the plane of the iron exhibit the most pronounced chemical shift differences. For example, the chemical shift of the imine methyl group for the dinitrogen complexes is centered at 13.45 ppm at 20 °C, whereas in **1-(CO)$_2$** this peak appears at 2.12 ppm. Similar isotropic shifts are observed for the *meta* and *para* pyridine peaks. In contrast, the resonances for the orthogonal aryl groups have isotropic shifts approaching zero (see the Supporting Information).

(53) Sur, S. K. *J. Magn. Reson.* **1989**, *82*, 169.

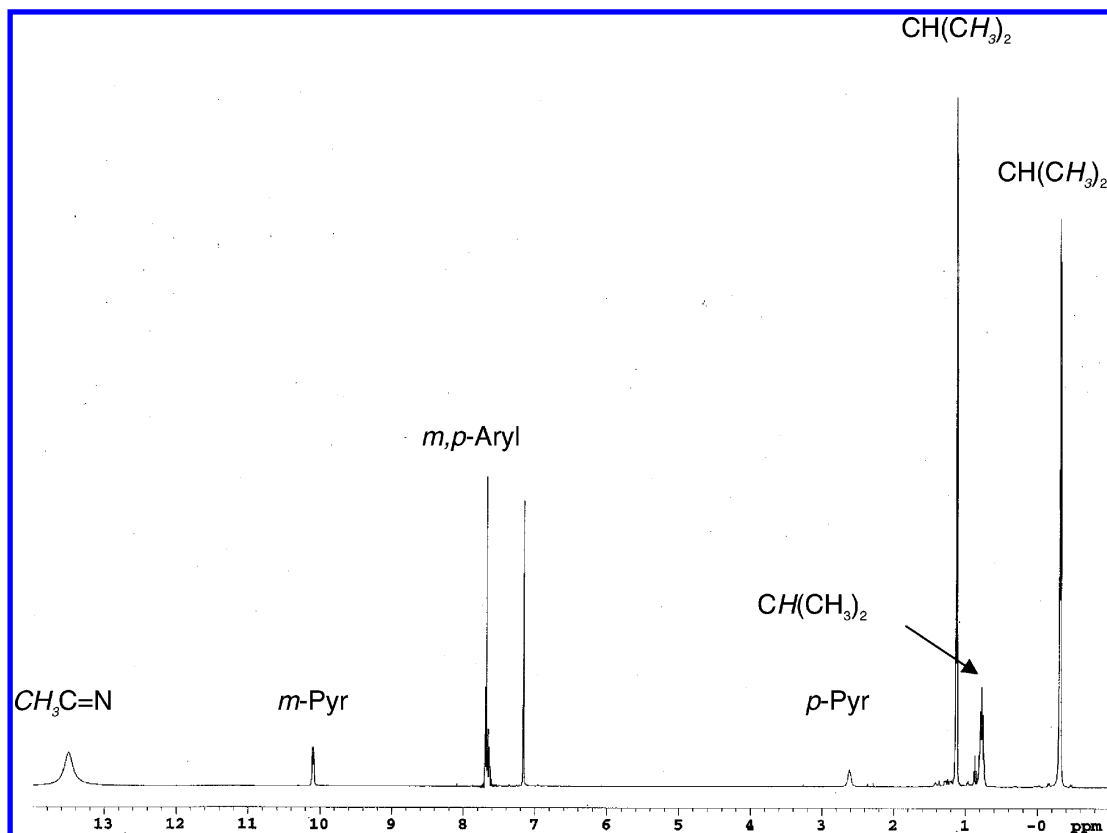(54) Gerloch, M.; Miller, J. R. *Prog. Inorg. Chem.* **1968**, *10*, 1.

Figure 3. ^{1}H NMR spectrum of **1-(N$_2$)$_2$/1-N$_2$** in benzene-d_6 at 22 °C.

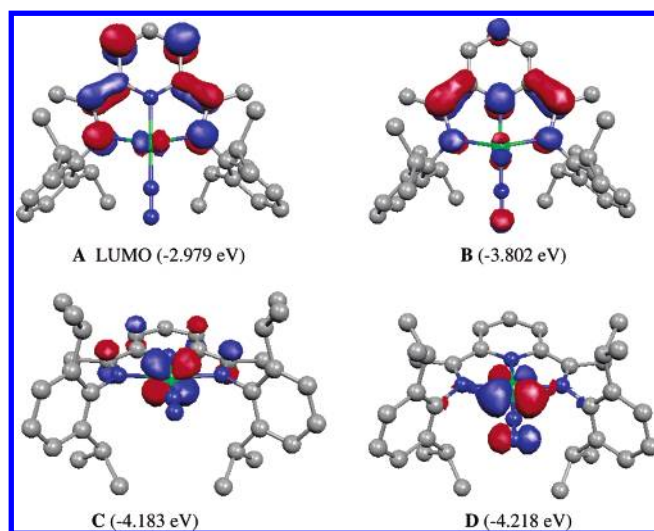**Figure 4.** Selected molecular orbitals of **1-N$_2$** (ADF2003.01, TZ2P, ZORA, α-spin formalism).

The electronic structures of **1-(N$_2$)$_2$**, **1-N$_2$**, and **1-(CO)$_2$** were investigated with density functional theory (ADF2003.01, TZ2P, ZORA) and account for the spin delocalization phenomenon and the observed isotropic shifts. Selected frontier molecular orbitals (α-spin formalism) of **1-N$_2$** are presented in Figure 4. Those for **1-(N$_2$)$_2$** and **1-(CO)$_2$** are contained in the Supporting Information. For both **1-N$_2$** and **1-(N$_2$)$_2$**, the LUMOs and one of the singly occupied orbitals (B) are principally the π-system of the PDI ligand that provides a pathway for the unpaired spin to delocalize from the iron center. Significant orbital coefficients are observed on the *para* pyridine carbon as well as on C=N, consistent with the larger isotropic shifts observed for these

hydrogens. In contrast, the orthogonal aryl groups provide no contribution to these orbitals, and as a result small isotropic shifts are observed.

Catalytic Activity of 1-(N$_2$)$_2$ in Homogeneous Hydrogenation. With a well-defined iron(0) complex containing labile N$_2$ ligands in hand, the catalytic activity of **1-(N$_2$)$_2$** was evaluated in carbon−hydrogen and carbon−silicon bond forming reactions.[55] Preliminary experiments revealed that **1-(N$_2$)$_2$** is an active precatalyst for the hydrogenation of simple olefins, such as 1-hexene and cyclohexene, to the corresponding alkanes at ambient temperature and 1 atm of H$_2$ (eq 4).
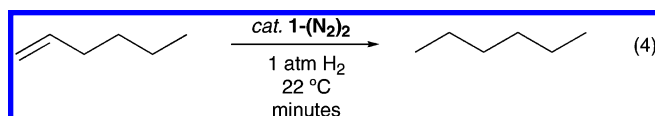
These results prompted a more systematic study of olefin hydrogenation. Each catalytic reaction was conducted using a 1.25 M solution of olefin in toluene containing 0.3 mol % **1-(N$_2$)$_2$** with 4 atm of hydrogen at 22 °C. The reactions can also be efficiently conducted at 1 atm of H$_2$; 4 atm was used to avoid potential complications in comparing relative rates at low hydrogen pressures. The results of the catalytic hydrogenation reactions are contained in Table 2. Terminal alkenes such as 1-hexene and styrene are hydrogenated to the corresponding alkanes with high activity, proceeding to completion within minutes under standard conditions. Internal and *gem*-disubstituted olefins are also effectively hydrogenated, although slightly longer reaction times are required to reach complete conversion.

(55) Although **1-(N$_2$)$_2$** loses 1 equiv of dinitrogen in solution, we will refer to the precatalyst as **1-(N$_2$)$_2$** throughout the paper as this is the compound that is isolated and charged into the catalytic reactions.

Table 2. Olefin Hydrogenation with 0.3 mol % **1-(N$_2$)$_2$**

Substrate	time (min)[a]	tof (mol/hr)[b]
	12	1814
Ph	16	1344
	380	57
Ph	210	104
	60	363
	210	104[c]
MeO$_2$C ... CO$_2$Me	360	3.3[d]

[a] Time required to reach >98% conversion as judged by GC. [b] Determined on the basis of the time required to reach completion. [c] The product is (+)-*p*-menth-1-ene. [d] A 5 mol % concentration of **1-(N$_2$)$_2$**.

Diolefins such as 1,5-hexadiene and (+)-(*R*)-limonene are also rapidly hydrogenated under standard conditions. The activity for 1,5-hexadiene is slightly reduced from 1-hexene, requiring 60 min rather than 12 min for complete consumption of the diolefin. Hydrogenation of (+)-(*R*)-limonene selectively yields (+)-*p*-menth-1-ene arising from preferential hydrogenation of the *gem*-disubstituted olefin over the trisubstituted alkene. Functionalized olefins such as dimethyl itaconate are also hydrogenated, although higher catalyst loadings of 5.0 mol % are required for comparable activity. Attempts to hydrogenate more hindered olefins such as 1-methylcyclohexene and tetramethylethylene under standard conditions have been unsuccessful, although conjugated dienes such as 1,3-butadiene, hindered terminal olefins such as *tert*-butylethylene, and internal olefins such as *trans*-2-hexene are also readily hydrogenated.
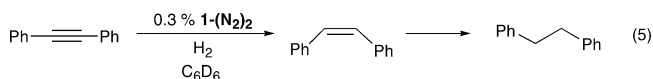
Preparative-scale olefin hydrogenation can also be carried out in neat alkene with high activity. For example, addition of 4 atm of H$_2$ to neat 1-hexene or cyclohexene with only 0.04 mol % (40 ppm) **1-(N$_2$)$_2$** allowed quantitative isolation of hexane or cyclohexane after 19 and 26 h, respectively. Importantly, the product can be easily separated from the catalyst by vacuum transfer. If nonvolatile, liquid substrates are used, the catalyst can be simply removed by exposing the reaction mixture to air and filtering away the oxidized iron byproduct. The high activity of **1-(N$_2$)$_2$** in nonpolar solvents or pure substrates contrasts the behavior of traditional precious-metal catalysts, which typically require polar solvents for optimal activity.[56,57] Hydrogenations in neat alkene were studied because solvent-free reactions are environmentally more attractive and obviate the need for product−solvent separation.[58]

Internal alkynes such as diphenylacetylene are also effectively hydrogenated with **1-(N$_2$)$_2$**. Monitoring the catalytic hydrogenation reaction in situ by ¹H NMR spectroscopy revealed initial, selective formation of *cis*-stilbene followed by complete conversion to bibenzyl (eq 5). Other internal alkynes such as 2-butyne can also be hydrogenated, initially producing *cis*-2-butene and ultimately yielding butane. Attempts to hydrogenate terminal

Table 3. Comparison of **1-(N$_2$)$_2$** with Traditional Precious Metal Catalysts for the Hydrogenation of 1-Hexene

catalyst	time (min)	tof (mol/h)	catalyst	time (min)	tof (mol/h)
1-(N$_2$)$_2$	12	1814	(PPh$_3$)$_3$RhCl	12	10
10% Pd/C	12	366	[(COD)Ir(PCy$_3$)py]PF$_6$	12	75

alkynes such as trimethylsilylacetylene have not been successful, producing a number of unidentified organic products.

$$Ph\text{—}\!\!\equiv\!\!\text{—}Ph \xrightarrow[\substack{H_2 \\ C_6D_6}]{0.3 \% \text{ } \mathbf{1\text{-}(N_2)_2}} Ph\diagup\!\!\!\diagdown Ph \longrightarrow Ph\diagup\!\!\!\diagdown Ph \quad (5)$$

The high activity of **1-(N$_2$)$_2$** for the catalytic hydrogenation of olefins and alkynes prompted comparison with traditional precious metal catalysts. Developing a meaningful, quantitative comparison is difficult given that each catalyst operates under a different set of optimized conditions. Each catalytic reaction was carried out with 0.3 mol % metal complex in 4 mL of toluene with 1-hexene under 4 atm of H$_2$ at 22 °C for 12 min. The results from each catalytic experiment are reported in Table 3. The catalytic hydrogenations with (Ph$_3$P)$_3$RhCl produced only 7% hexane along with considerable amounts of internal hexenes arising from isomerization of the olefin. Crabtree's [(COD)Ir-(PCy$_3$)py]PF$_6$[59] and the ubiquitous heterogeneous catalyst 10% Pd/C are not as effective as **1-(N$_2$)$_2$** under these conditions. As stated previously, however, the precious metal catalysts are known to operate most effectively in polar solvents.

Catalytic Activity of 1-(N$_2$)$_2$ in Homogeneous Hydrosilation. The utility of **1-(N$_2$)$_2$** for catalytic hydrogenation prompted investigation into other types of carbon−element bond forming reactions involving insertion mechanisms. The hydrosilation of carbon−carbon multiple bonds is a powerful, atom-economical transformation that provides a flexible route to silanes and alcohols after appropriate oxidation.[60] While radical initiators[61] and Lewis acids[62] are known to promote hydrosilation, transition metal catalysis[63] has emerged as the preferred method due its high activity, selectivity, and in some cases stereospecificity.[64] Traditional hydrosilation catalysts contain precious metals such as platinum[65] or rhodium,[66] although several highly active group 3 transition metal[67] and lanthanide-based[68] catalysts have also been reported. In contrast, the development of well-defined homogeneous iron catalysts for hydrosilation has been quite limited. Iron carbonyl complexes such as Fe(CO)$_5$ hydrosilate simple olefins at high temperature, with significant dehydrogenative hydrosilation accompanying saturated alkylsilane formation.[69] Since this seminal discovery, the selective dehy-

(56) Schrock, R. R.; Osborn, J. A. *J. Am. Chem. Soc.* **1971**, *93*, 3091.
(57) Betley and Peters have reported a class of rhodium complexes that maintain their activity in nonpolar media: Betley, T. A.; Peters, J. C. *Angew. Chem., Int. Ed.* **2003**, *42*, 2385.
(58) Kimmich, B. F. M.; Fagan, P. J.; Hauptman, E.; Bullock, R. M. *Chem. Commun.* **2004**, 1014.
(59) Crabtree, R. H. *Acc. Chem. Res.* **1979**, *12*, 331.
(60) Hiyama, T.; Kusumoto, T. In *Comprehensive Organic Synthesis*; Trost, B. M., Fleming, I., Eds.; Pergamon Press: Oxford, 1991.
(61) Dohmaru, T.; Nagata, T.; Tsurugi, J. *Chem. Lett.* **1973**, 1031.
(62) (a) Song, Y.-S.; Yoo, B. R.; Lee, G. H.; Jung, I. N. *Organometallics* **1999**, *18*, 3109. (b) Yamamoto, K.; Takemae, M. *Synlett* **1990**, 259.
(63) Marciniec, B. *Comprehensive Handbook on Hydrosilation*; Pergamon: Oxford, 1992.
(64) Bosnich, B. *Acc. Chem. Res.* **1998**, *31*, 667.
(65) Speier, J. L. *Adv. Organomet. Chem.* **1977**, *17*, 407.
(66) Chalk, A. J. *J. Organomet. Chem.* **1970**, *21*, 207.
(67) For representative examples see: (a) Molander, G. A.; Dowdy, E. D.; Noll, B. C. *Organometallics* **1998**, *17*, 3754. (b) Molander, G. A.; Knight, E. E. *J. Org. Chem.* **1998**, *63*, 7009.
(68) Fu, P. F.; Brard, L.; Li, Y.; Marks, T. J. *J. Am. Chem. Soc.* **1995**, *117*, 7157.
(69) Nesmeyanov, A. N.; Freidlina, R. K.; Chukovskaya, E. C.; Petrova, R. G.; Belyavsky, A. B. *Tetrahedron* **1962**, *17*, 61.
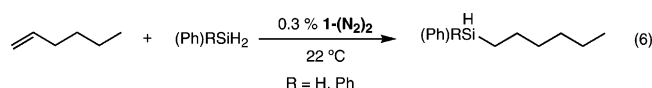
Table 4. Olefin Hydrosilation with Catalytic **1-(N$_2$)$_2$**

Substrate	Product	time (min)[a]	tof (mol/hr)[b]
	PhH$_2$Si⌒⌒⌒	60	364
Ph	Ph / PhH$_2$Si	90	242
	PhH$_2$Si⌒⌒⌒	4200	.09[c]
	SiH$_2$Ph	930	23
Ph	Ph / PhH$_2$Si	210	104
	PhH$_2$Si⌒⌒⌒SiH$_2$Ph	1110	20
	SiH$_2$Ph	120	182

^{a} Time required to reach >98% conversion as judged by GC. ^{b} Determined on the basis of the time required to reach completion. ^{c} 25% of the internal hydrosilation product was also obtained.
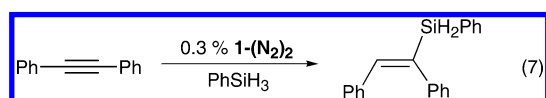
drogenative hydrosilation of styrene derivatives promoted by Fe$_3$(CO)$_{12}$ has also been described.[70]

Reaction of 1-hexene with either PhSiH$_3$ or Ph$_2$SiH$_2$ in the presence of 0.3 mol % **1-(N$_2$)$_2$** produced rapid hydrosilation over the course of minutes at 22 °C (eq 6). In both cases, the anti-Markovnikov product was formed exclusively and the hydrosilation with PhSiH$_3$ proceeded much faster than the corresponding reaction with Ph$_2$SiH$_2$.

$$\diagup\diagdown\diagup\diagdown \ + \ (Ph)RSiH_2 \xrightarrow[\substack{22\ ^\circ C \\ R = H, Ph}]{0.3\ \%\ \mathbf{1\text{-}(N_2)_2}} (Ph)RSi\diagdown\diagup\diagdown\diagup\diagdown \quad (6)$$

On the basis of these results, the ambient temperature hydrosilation of a series of olefins was examined using 1 equiv of PhSiH$_3$ in pentane solution in the presence of 0.3 mol % **1-(N$_2$)$_2$**. The progress of each reaction was monitored by gas chromatography and the identity of each hydrosilation product determined by multinuclear NMR spectroscopy and by comparison of GC traces of authentic samples. The results of this study are presented in Table 4. The relative rates of hydrosilation follow the same trend as those of hydrogenation, where terminal alkenes such as 1-hexene and styrene react most rapidly followed by *gem*-disubstituted olefins and internal olefins. In the case of *trans*-2-hexene, the terminally functionalized product predominates, although significant quantities (~25%) of internal silanes are also obtained. Significantly, no products arising from dehydrogenative hydrosilation were observed.

The hydrosilation of alkynes was also examined and proceeds efficiently under mild conditions. Addition of PhSiH$_3$ to Ph-C≡CPh produced the corresponding silylolefin in quantitative yield (eq 7). Reaction with excess silane was not observed even in the presence of large excesses (>5 equiv) due to steric hindrance of the resulting silylalkene.

$$Ph\!\!-\!\!\!\equiv\!\!\!-\!\!Ph \xrightarrow[PhSiH_3]{0.3\ \%\ \mathbf{1\text{-}(N_2)_2}} \begin{array}{c} SiH_2Ph \\ Ph \diagup\diagdown Ph \end{array} \quad (7)$$

(70) Kakiuchi, F.; Tanaka, Y.; Chatani, N.; Murai, S. *J. Organomet. Chem.* **1993**, *456*, 45.
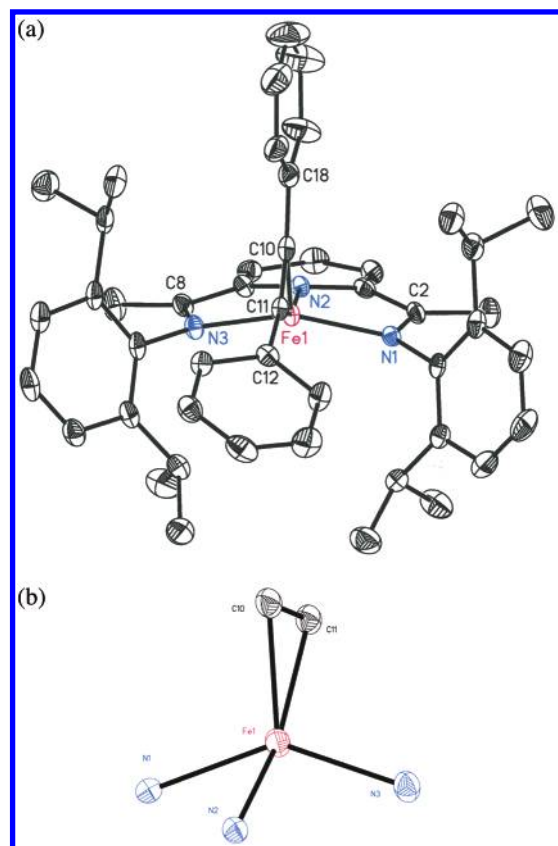
Figure 5. (a) Molecular structure of **1-(PhC≡CPh)** (30% probability ellipsoids). Hydrogen atoms omitted for clarity. (b) View of the core of the molecule.

Synthesis and Characterization of Potential Catalytic Intermediates. In an attempt to gain a better understanding of the mechanisms of both catalytic hydrogenation and hydrosilation, several stoichiometric reactions with **1-(N$_2$)$_2$** were conducted. One observation was that the catalytic reactions undergo a striking color change from green to red upon addition of olefin or alkyne. Mixing 1 equiv of PhC≡CPh and solid **1-(N$_2$)$_2$** followed by addition of pentane resulted in liberation of 2 equiv of dinitrogen (confirmed by Toepler pump analysis) and formation of a red solution. Recrystallization at −35 °C allowed isolation of red crystals identified as the alkyne complex **1-(PhC≡CPh)** (eq 8). Significantly, independently prepared **1-(PhC≡CPh)** is catalytically competent for both olefin hydrogenation and hydrosilation with turnover frequencies identical to those of **1-(N$_2$)$_2$**.
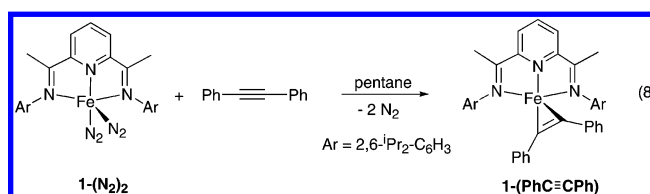
The solid-state structure of **1-(PhC≡CPh)** was determined by single-crystal X-ray diffraction and is shown in Figure 5. Selected bond distances and angles are presented in Table 5. In viewing the structure of **1-(PhC≡CPh)**, it is apparent that the overall geometry of the molecule has changed dramatically from that of **1-(N$_2$)$_2$**. Both the iron atom and the carbon of the alkyne ligand, C(11), are significantly displaced from the plane defined

Table 5. Selected Bond Distances and Angles for **1-(PhC≡CPh)**

|	distance (Å)		angle (deg)
C(10)−C(11)	1.283(6)	C(10)−Fe(1)−C(11)	38.55(19)
Fe(1)−C(10)	1.934(5)	C(10)−C(11)−C(12)	153.1(5)
Fe(1)−C(11)	1.952(5)	C(11)−C(10)−C(18)	147.2(5)
Fe(1)−N(1)	2.039(4)	N(1)−Fe(1)−N(2)	77.89(15)
Fe(1)−N(2)	1.908(4)	N(2)−Fe(1)−N(3)	78.06(15)
Fe(1)−N(3)	2.039(4)	N(1)−Fe(1)−N(3)	143.37(15)
N(1)−C(2)	1.326(6)		
N(3)−C(8)	1.326(6)		
deviation of Fe(1)[a]	0.587		
deviation of C(11)[a]	1.794		

[a] Deviation from the plane defined by N(1)−N(2)−N(3).

by the three nitrogens of the PDI ligand (Table 5). Applying the Dewar−Chatt−Duncanson model for olefin coordination,[71] **1-(PhC≡CPh)** can be described either as a distorted five-coordinate Fe(II) complex or as a pseudotetrahedral iron(0) compound. The carbon−carbon bond length of the coordinated alkyne is 1.283(6) Å, significantly elongated from the C≡C bond length of 1.210(3) Å reported for free PhC≡CPh,[72] and is consistent with considerable π-back-bonding from the iron center.

The molecular structure of **1-(PhC≡CPh)** also provides insight into the nature of substrate−catalyst interaction. In addition to the previously noted deviation in molecular geometry, the phenyl ring attached to C(10) is oriented almost perpendicular to the iron−^{iPr}PDI ligand plane, most likely to avoid unfavorable steric interactions with the isopropylaryl groups flanking the iron atom. In contrast, the phenyl substituent attached to C(11) lies nearly parallel to the ligand plane and is significantly rotated with respect to the other phenyl substituent, nestled between the two aryl rings of the PDI ligand.

Solution magnetic measurements also support the Fe(0)/Fe(II) bonding description. The magnetic moment in benzene-d_6 at 22 °C was found to be 2.71 μ_B, in reasonable agreement with the spin-only value for an $S = 1$ molecule. Two unpaired electrons are consistent with both a formally d^8 tetrahedral Fe(0) complex or an intermediate spin d^6 Fe(II) compound. Unlike **1-N₂**, the ^{1}H NMR spectrum of **1-(PhC≡CPh)** is broad and featureless and has not proven useful for characterization. This behavior is most likely due to the displacement of the iron atom from the ligand plane, reducing the overlap required for conjugation with the pyridinimine π-system, thereby placing the unpaired spins in iron-based d-orbitals.

Provided the activity of **1-(N₂)₂** for catalytic hydrogenation and hydrosilation, the stoichiometric reactions of the iron bis(dinitrogen) complex with H₂ and silanes were also investigated. Stirring a pentane solution of **1-(N₂)₂** with excess PhSiH₃ followed by recrystallization at −35 °C afforded a green crystalline solid identified as the iron(0) bis(silane) complex (^{iPr}PDI)Fe(η^2-SiH₃Ph)₂ (**1-(Si)₂**) (eq 9). The solution magnetic moment was determined in benzene-d_6 at 22 °C and found to

(9)

1-(N₂)₂   **1-(Si)₂**
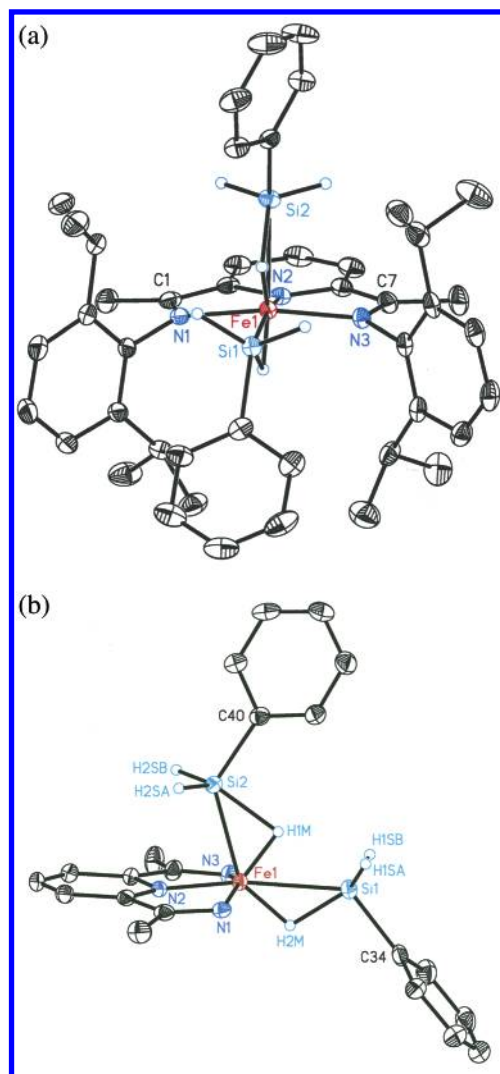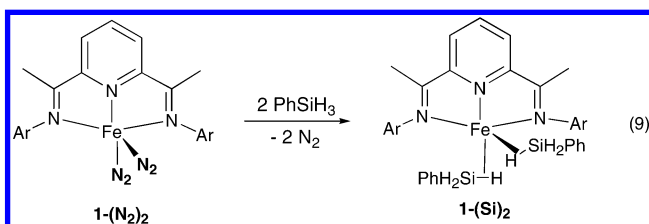
Figure 6. (a) Molecular structure of **1-(Si)₂** (30% probability ellipsoids). Hydrogen atoms, except silane hydrogens, and cocrystallized pentane molecule omitted for clarity. (b) View of the core of the molecule.

be 2.68 μ_B, consistent with an $S = 1$ high spin, five-coordinate Fe(0) complex. Isolated **1-(Si)₂** is an effective precatalyst for the hydrosilation of 1-hexene.

The solid-state structure of **1-(Si)₂** was determined by X-ray diffraction, and the molecular structure is shown in Figure 6. Accompanying selected bond distances and angles are reported in Table 6. The data were of sufficient quality such that all of the hydrogen atoms were located and freely refined. The geometry of the molecule is similar to that of **1-(N₂)₂** and is best described as distorted square pyramidal with basal and apical silane ligands. As with **1-(N₂)₂**, the iron atom is nearly coplanar with the three nitrogens of the ^{iPr}PDI ligand being raised out of the plane by 0.260 Å. The basal silicon is raised out of the plane by 0.209 Å, more so than the basal N₂ ligand in **1-(N₂)₂**. This distortion is most likely a consequence of the σ-coordination of the bulky silane as compared to linear N₂. The phenyl rings of the silane ligands adopt an orientation similar to that observed in the alkyne adduct **1-(PhC≡CPh)**. The basal phenyl ring lies essentially in the pocket formed by

(71) Miessler, G. L.; Tarr, D. A. *Inorganic Chemistry*, 3rd ed.; Prentice Hall: Upper Saddle River, NJ, 2004; p 482.
(72) Zanin, I. E.; Antipin, M. Y.; Struchkov, Y. T. *Kristallografiya* **1991**, *36*, 411.

Table 6. Selected Bond Distances and Angles for **1-(Si)$_2$**

	distance (Å)		angle (deg)
Fe(1)−H(1M)	1.45(3)	Fe(1)−Si(1)−H(2M)	35.8(9)
Fe(1)−H(2M)	1.51(3)	Fe(1)−Si(2)−H(1M)	38.5
Fe(1)−Si(1)	2.4733(7)	H1SA−Si(1)−H1SB	111.3(14)
Fe(1)−Si(2)	2.3266(8)	H2SA−Si(2)−H2SB	105.7(15)
Si(1)−H2(M)	1.59(2)	H2M−Si(1)−C(34)	95.8(9)
Si(2)−H1(M)	1.82(3)		
Si(1)−H1SA	1.41(2)	N(1)−Fe(1)−N(2)	79.61(9)
Si(1)−H1SB	1.39(2)	N(2)−Fe(1)−N(3)	79.52(8)
Si(2)−H2SA	1.33(2)	N(1)−Fe(1)−N(3)	155.62(8)
Si(2)−H2SB	1.38(2)	N(2)−Fe(1)−Si(1)	170.69(7)
Fe(1)−N(1)	1.9550(19)	N(2)−Fe(1)−Si(2)	80.97(6)
Fe(1)−N(2)	1.8399(19)		
Fe(1)−N(3)	1.9525(19)		
N(1)−C(1)	1.334(3)		
N(3)−C(7)	1.327(3)		
deviation of Fe(1)[a]	0.260		
deviation of Si(1)[a]	0.209		

[a] Deviation from the plane defined by N(1)−N(2)−N(3).

the isopropylaryl groups, while the apical phenyl group is again oriented to avoid steric interactions with the flanking isopropyl groups and is slightly twisted from the plane defined by Si(1)−Fe(1)−Si(2).

The silicon−hydrogen distance of the basal σ-complexed silane is slightly elongated to 1.59(2) Å in comparison to the values of 1.39(3) and 1.41(2) Å for the free silicon hydrogens, values in good agreement with those of free silanes.[73] The apical σ-complexed silicon−hydrogen bond shows much greater elongation with a bond length of 1.82(3) Å in comparison to free Si−H bond lengths of 1.38(2) and 1.33(2) Å. The longer apical silicon−hydrogen bond may result from greater overlap of the iron d_{xz} and d_{yz} orbitals with the Si−H σ*-orbital. The iron−silicon bond lengths (Table 6), while typically not a reliable measure of σ-complexation, are within the range typically found in iron σ-complexes.[74]

The solution structure of **1-(Si)$_2$** was elucidated by multinuclear NMR spectroscopy. Unlike **1-(N$_2$)$_2$**, both silane ligands in **1-(Si)$_2$** are retained in solution, demonstrating the higher affinity of the L$_3$Fe(0) fragment for silane σ-complexation over coordination of N$_2$. At 20 °C, benzene-d_6 solutions of **1-(Si)$_2$** exhibit broadened resonances that are a result of either paramagnetism or ligand exchange dynamics that are on the time scale of the NMR experiment.

Cooling a toluene-d_8 sample to temperatures below −20 °C produces sharp signals that display $^3J_{HH}$ coupling. Importantly, the chemical shifts of these resonances do not change dramatically as is observed for **1-N$_2$**, suggesting that the broadening observed at room temperature is due to a dynamic process rather than paramagnetism. Low temperature, static spectra of **1-(Si)$_2$** display C_s molecular symmetry consistent with the solid-state structure, which contains an idealized mirror plane of symmetry bisecting the basal silane ligand. Complete assignment of each ^{iPr}PDI ligand resonance was accomplished by gCOSY and ROESY NMR experiments, the full details of which can be found in the Experimental Section. Over all temperatures studied, two resonances upfield of SiMe$_4$ are observed at −0.02 and −7.02 ppm and assigned to the σ-complexed Si−H bonds.

A NOESY experiment, in conjunction with the ROESY data, was used to definitively assign the apical and basal ligands.

The resonance centered at −0.02 ppm exhibits cross-peaks with the ligand isopropyl groups, while the resonance centered at −7.02 ppm displays no through-space interactions with the aryl rings. On the basis of these data, the peak at −0.02 ppm is assigned to the apical silane, whereas the resonance at −7.02 ppm corresponds to the basal silane. The observation of C_s ligand symmetry in combination with two distinct silane environments clearly establishes a higher barrier for intramolecular dynamics than is observed for **1-(CO)$_2$** and **1-Cl$_2$**.[16] Applying the rocking mechanism suggested for **1-(CO)$_2$**, a higher barrier for **1-(Si)$_2$** would be anticipated due to the larger, three-dimensional features of the silane ligands.

A two-dimensional ^{1}H−^{29}Si HMBC experiment was also conducted to correlate the η^2-Si−H bonds with the appropriate free Si−H resonances. The data clearly establish that the singlet observed at 2.73 ppm corresponds to the uncomplexed Si−H bonds from the apical silane at −0.02 ppm whereas the singlet at 6.03 ppm corresponds to the basal silane resonating at −7.02 ppm. The remaining assignments for **1-(Si)$_2$** can be found in the Experimental Section.

Additional information regarding the solution structure of **1-(Si)$_2$** was obtained from one-dimensional ^{29}Si NMR spectroscopy. The ^{29}Si NMR spectrum was recorded at −80 °C and exhibited two sets of resonances for the inequivalent silane ligands (Figure 7). The first, centered at 50.23 ppm, displays coupling to both the terminal Si−H bonds and the silicon−hydrogen bond engaged in bonding to the iron center. From this peak, $^1J_{SiH}$ coupling constants of 54 and 196 Hz were measured for the η^2-Si−H and free Si−H bonds, respectively. The second ^{29}Si resonance, centered at −44.58 ppm, yielded larger coupling constants of 119 and 220 Hz for the bound and free silicon hydrogens, respectively. The values of the $^1J_{SiH}$ coupling constants are well within the range typically assigned to silane σ-complexes[74,75] and indicate that in solution **1-(Si)$_2$** is best viewed as a high spin, d^8 distorted square pyramidal iron complex. This formulation is in agreement with both the solid-state structure and the crystal structure observed for **1-(N$_2$)$_2$**. Moreover, the larger $^1J_{SiH}$ coupling constant observed for the basal silane ligand is consistent with the shorter Si−H bond observed in the solid-state structure.

While several iron silane σ-complexes have been reported, most are dinuclear.[74] Thus, structural characterization of **1-(Si)$_2$** is a rare example of a mononuclear iron bis(silane) complex.[76] Monomeric phosphine complexes such as ((^{n}Bu)Ph$_2$P)$_3$FeH$_3$-SiMePh$_2$[77] and (dppe)(CO)$_2$Fe(H)SiR$_3$ (dppe = diphenylphosphinoethane; R = OMe, OEt, Me)[78] have been reported previously and characterized in solution by NMR spectroscopy. Variable-temperature NMR experiments demonstrated the fluxional behavior of these molecules.

The analogous reactivity of **1-(N$_2$)$_2$** with dihydrogen was also explored. Exposure of a benzene-d_6 solution of **1-(N$_2$)$_2$** to 1 atm of H$_2$ produced a brown solution. Analysis by ^{1}H NMR spectroscopy revealed complete consumption of the starting dinitrogen complex with concomitant growth of a new C_{2v}

(73) Kawachi, A.; Tanaka, K.; Tamao, K. *Organometallics* **1997**, *16*, 5102.

(74) Corey, J. Y.; Braddock-Wilking, J. *Chem. Rev.* **1999**, *99*, 175.
(75) Schubert, U. *Adv. Organomet. Chem.* **1990**, *30*, 151.
(76) Other bis(silane) complexes: (a) (Ru) Delpech, F.; Sabo-Etienne, S.; Chaudret, B.; Daran, J.-C. *J. Am. Chem. Soc.* **1997**, *119*, 3167. (b) (Ir) Luo, X.-L.; Crabtree, R. H. *J. Am. Chem. Soc.* **1989**, *111*, 2527.
(77) Schubert, U.; Gilbert, S.; Mock, S. *Chem. Ber.* **1992**, *36*, 2628.
(78) Gilbert, S.; Knorr, M.; Mock, S.; Schubert, U. *J. Organomet. Chem.* **1994**, *480*, 241.
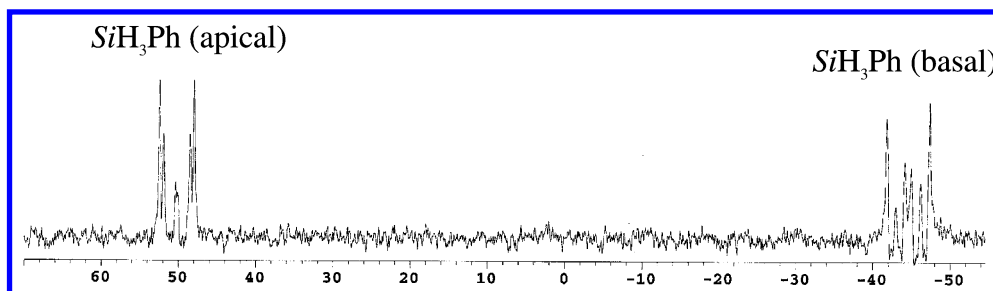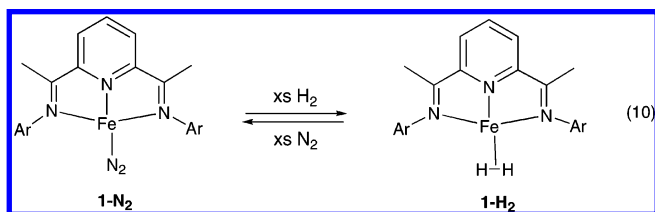
Figure 7. ^{29}Si NMR spectrum of **1-(Si)$_2$** at −80 °C in toluene-d_8.

symmetric product with spectral features nearly identical to those of **1-N$_2$**. On the basis of the NMR data, elemental analysis, isotopic labeling, and Toepler pump analysis, the product is assigned as the iron(0) dihydrogen complex **1-H$_2$** (eq 10).

While all of the ligand resonances are observed and can be readily assigned (Experimental Section), signals attributable to the dihydrogen ligands have not been located. Attempts to observe IR bands for the dihydrogen (or dideuterium) ligand have also been unsuccessful. Addition of even trace amounts of N$_2$ to **1-H$_2$** results in rapid displacement of the dihydrogen molecule and quantitative regeneration of **1-N$_2$**. This extreme nitrogen sensitivity makes handling and isolating pure **1-H$_2$** challenging. Comparison of the relative stability of each iron-(0) compound allows ordering of the ligand preferences for the (^{iPr}PDI)Fe(0) fragment as PhSiH$_3$ > N$_2$ > H$_2$.

The solution magnetic susceptibility of **1-H$_2$** was determined in benzene-d_6 and found to be 2.70 μ_B at 22 °C, consistent with an $S = 1$ ground state. This value, taken in conjunction with the NMR data, suggests that the structure of **1-H$_2$** is similar to that of **1-N$_2$**, although an iron(II) dihydride cannot be definitively excluded. Presumably the electron-withdrawing character of the ^{iPr}PDI ligand renders the iron center sufficiently electron deficient to inhibit oxidative addition of either H$_2$ or silane. Significantly, isolated samples of **1-H$_2$** are competent for the catalytic hydrogenation of olefins and alkynes with activities similar to those of **1-(N$_2$)$_2$**.

Preparation of the corresponding bis(deuterium) complex **1-D$_2$** was accomplished by addition of 1 atm of D$_2$ gas to **1-(N$_2$)$_2$**. Monitoring benzene solutions of the organometallic product by ^{2}H NMR spectroscopy as a function of time did not result in location of the η^2-D$_2$ ligands but was effective in demonstrating selective deuterium incorporation into the isopropyl methyl groups. The exchange process takes place over the course of several days at ambient temperature and is much slower than the time scale of a catalytic hydrogenation reaction. A proposed mechanism that accounts for the experimental observations is presented in the Supporting Information. Although many pathways involving a range of intermediates are possible, we favor loss of the η^2-D$_2$ ligands to form a five-coordinate, 16-electron iron(II) cyclometalated hydride, in analogy to **1-Cl$_2$**.[16,17] Exchange of the hydride for the deuteride by σ-bond metathesis
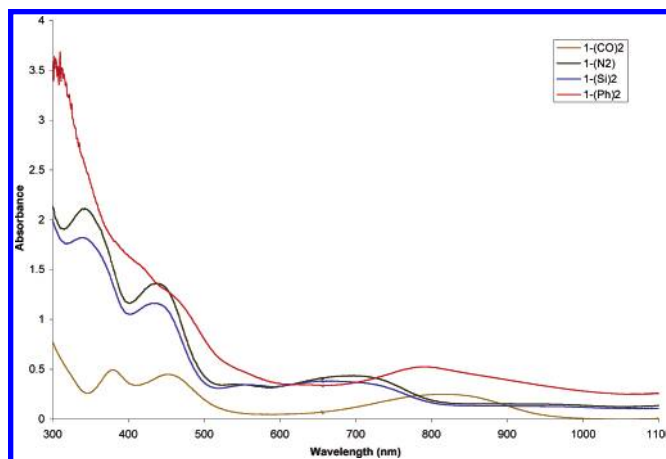

Figure 8. Electronic spectra of **1-N$_2$**, **1-(CO)$_2$**, **1-(Si)$_2$**, and **1-(PhC≡CPh)** recorded in pentane at 22 °C.

Table 7. Absorption Maxima (nm) and Extinction Coefficients for the Series of Fe(0) Compounds

1-N$_2$		1-(N$_2$)$_2$	1-(CO)$_2$		1-(Si)$_2$		1-(PhC≡CPh)	
$\lambda_{max}{}^a$	ϵ	$\lambda_{max}{}^b$	λ_{max}	ϵ	λ_{max}	ϵ	λ_{max}	ϵ
342	9000	458	379	3600	342	13,000	414	2800
423	6700	634	452	3300	430	9900	468	2000
657	2000	883	817	1800	560	3500	789	1000
950	790				685	3300		
					916	790		

^{a} Measured in nanometers. References: λ_{max}(^{iPr}PDI) = 354 nm, λ_{max}-(**2-Cl$_3$**) = 370 nm. ^{b} Spectrum recorded at −78 °C.

or an oxidative addition−reductive elimination sequence produces isotopic exchange. Subsequent reductive elimination of a C−D bond generates the observed product.

Electronic Spectra of (^{iPr}PDI)Fe(0) Complexes. The electronic structure of the series of iron(0) compounds reported in this work was investigated by UV−vis spectrophotometry. To aid with spectral assignment, the synthesis of an ^{iPr}PDI metal complex that would not be complicated by d−d transitions or MLCT bands was targeted. For this reason, (^{iPr}PDI)ScCl$_3$ (**2-Cl$_3$**) was prepared and crystallographically characterized and its electronic spectrum recorded (see the Supporting Information).

Variable temperature electronic spectroscopy provided additional evidence for the reversible dissociation and recoordination of dinitrogen from **1-(N$_2$)$_2$**. The spectrum of **1-N$_2$** recorded at 22 °C in pentane is presented in Figure 8 and exhibits four bands (Table 7). Upon cooling to −78 °C, these bands disappear at the expense of three new bands that are assigned to the five-coordinate, bis(dinitrogen) complex **1-(N$_2$)$_2$**. This behavior is in agreement with the in situ solution IR data. Band assignments, while tentative, are based on spectra recorded

for the free ligand, **2-Cl₃**, and literature data.[17,18] For **1-N₂**, charge-transfer bands centered at 342 and 423 nm are observed along with strong intensity-stealing MLCT bands centered at 657 nm.[79] A weaker d–d transition is observed at 950 nm. Similar features are observed for **1-(CO)₂** and **1-(Si)₂** (Figure 8, Table 7). In these molecules, the d–d bands most likely arise from the dipole- and spin-allowed $^3B_1 \rightarrow {}^3E$ transition typically observed for isoelectronic $S = 1$, square pyramidal Ni(II) d^8 complexes.[51]

The electronic spectrum of **1-(PhC≡CPh)** (Figure 8) reflects the structural difference of the molecule as compared to **1-(CO)₂** or **1-(Si)₂**. Recall that the iron atom in **1-(PhC≡CPh)** is displaced significantly from the basal plane, resulting in a pseudotetrahedral rather than a square pyramidal iron(0) center. The intraligand-charge-transfer band is red shifted significantly and has a much lower extinction coefficient than that of the square pyramidal compounds. Likewise, weaker intensity MLCT bands are also observed at 468 and 789 nm. No bands assignable to d–d transitions were located.

Isotopic Labeling Studies and Mechanistic Insights. A series of isotopic labeling studies was also performed with the intent of providing additional mechanistic insight into iron-catalyzed hydrogenation and hydrosilation. The stereochemistry of initial hydrogen addition was established by addition of D₂ to an olefin, where isotopic scrambling is prohibited by restricted β-hydrogen elimination. Deuteriolysis of norbornene in the presence of catalytic **1-(N₂)₂** afforded *exo,exo-2,3-d₂*-norbornane exclusively, consistent with *syn* addition of D₂ (H₂) (eq 11).[80] This result is also in agreement with the observation of *cis*-stilbene as the sole organic intermediate in the hydrogenation of diphenylacetylene to bibenzyl.
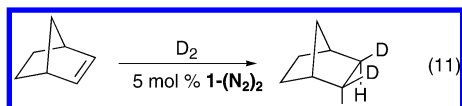
The addition of D₂ to alkenes that could participate in facile β-hydrogen elimination and subsequent "chain running" processes was also investigated. Deuteriolysis of 1-butene with 5 mol % **1-(N₂)₂** rapidly afforded butane-*d₂* in quantitative yield (eq 12).
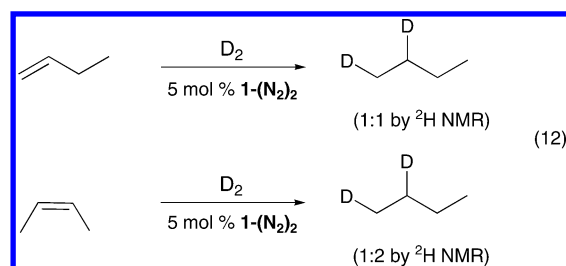

Analysis of the product by ^{2}H NMR spectroscopy revealed a 1:1 ratio of the isotopic label in the terminal and internal positions of the butane-*d₂*, indicating that terminal olefins do not undergo competitive chain running processes. This result also demonstrates that the olefin inserts solely in a 1,2-fashion and that isomerization of the iron *n*-alkyl hydride to the *sec*-alkyl hydride is not competitive on the time scale of the catalytic

hydrogenation reaction. The analogous experiment with *cis*-2-butene also provided butane-*d₂*; however, a 2:1 ratio of internal to terminal deuterium was observed in this case. The migration of the deuterium label from the internal to the terminal position demonstrates the proclivity of internal olefins to participate in alkyl migrations during catalytic hydrogenation. This behavior is reminiscent of group 4 metallocene alkyl hydride complexes, where internal alkyls undergo facile chain isomerization and isotopic scrambling reactions, while terminal alkyls do not.[81]

As reported in an earlier section, treatment of **1-(N₂)₂** with D₂ gas resulted in isotopic exchange of the isopropyl methyl substituents arising from reversible cyclometalation. To determine whether this process is competitive with olefin hydrogenation, the catalytic deuteriolysis of 1-hexene was performed. After the reaction was complete, the hexane-*d₂* was removed and the catalyst solution was treated with 1 atm of CO to generate diamagnetic **1-(CO)₂**. Analysis of this compound by ^{2}H NMR spectroscopy revealed no deuterium incorporation into the ligand, demonstrating that cyclometalation is not competitive with terminal olefin hydrogenation.

Addition of excess olefin to **1-(N₂)₂** without dihydrogen or silane produced red solutions, most likely due to the formation of olefin complexes in analogy to isolated **1-(PhC≡CPh)**. Allowing solutions containing 1-butene to stand at ambient temperature in the presence of catalytic **1-(N₂)₂** resulted in net alkene isomerization to yield an equilibrium mixture of *cis*- and *trans*-2-butene. Similar results were also obtained for 1-hexene, where a mixture of 2- and 3-hexenes is observed (eq 13). Quantitation of the internal hexenes was not possible due to overlapping resonances in the ^{1}H NMR spectrum.
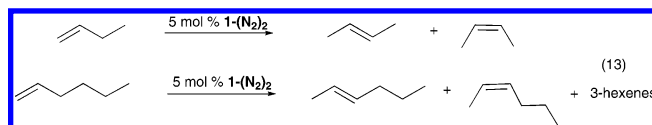
Samples of pure internal olefins such as *cis*- and *trans*-2-butene isomerize in the presence of catalytic amounts **1-(N₂)₂** to an equilibrium mixture of 2-butenes (eq 14).
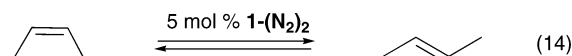
It is important to note that the rate of terminal olefin isomerization is much slower than that of catalytic hydrogenation or hydrosilation. Internal olefins are not observed during the course of the catalytic reaction. While a detailed mechanistic investigation of olefin isomerization promoted by **1-(N₂)₂** is currently under investigation, we favor an allyl hydride intermediate originally proposed by Casey and Cyr for similar reactions promoted by Fe(CO)₅.[82]

A mechanism consistent with the experimental data collected is presented in Figure 9. Loss of 2 equiv of N₂ from **1-(N₂)₂** (or alternatively 1 equiv from **1-N₂**) affords the active L₃Fe(0) fragment. The next step, olefin coordination, is preferred over oxidative addition of H₂ given the extreme nitrogen sensitivity of **1-H₂** and observation and crystallographic characterization

(79) Harris, D. C.; Bertolucci, M. D. *Symmetry and Spectroscopy: An Introduction to Vibrational and Electronic Spectroscopy*; Dover: New York, 1978; Chapter 5.
(80) Marchand, A. P.; Marchand, N. W. *Tetrahedron Lett.* **1971**, *18*, 1365.
(81) Chirik, P. J.; Day, M. D.; Labinger, J. A.; Bercaw, J. E. *J. Am. Chem. Soc.* **1999**, *121*, 10308.
(82) Casey, C. P.; Cyr, C. R. *J. Am. Chem. Soc.* **1973**, *95*, 2248.
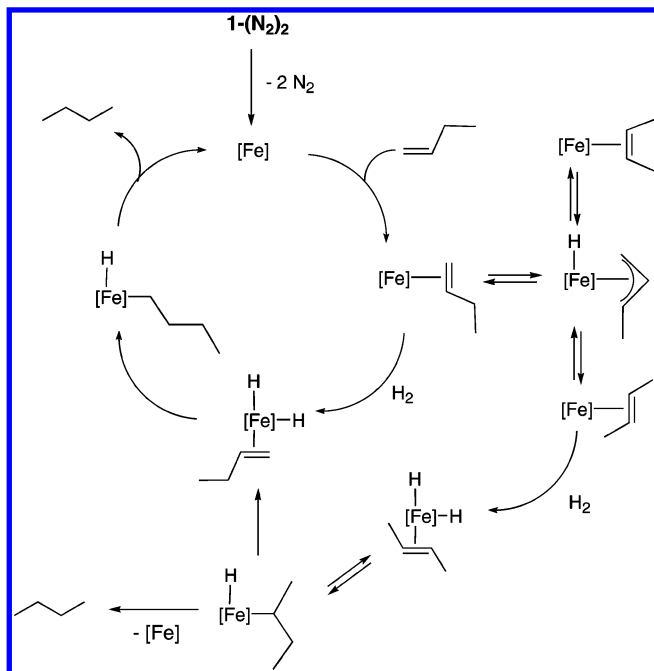
Figure 9. Proposed mechanism for catalytic hydrogenation with **1-(N$_2$)$_2$**.

of **1-(PhC≡CPh)**. However, this anecdotal evidence does not definitively exclude an iron(II) dihydride in the catalytic cycle.

Following olefin coordination, oxidative addition of H$_2$ provides a formally 18-electron olefin dihydride intermediate. Olefin insertion and subsequent alkane reductive elimination afford the alkane product and regenerate the L$_3$Fe(0) fragment. Isotopic labeling studies establish chain running in internal olefins that accompanies hydrogenation, suggesting competitive β-hydrogen elimination of the intermediate iron *sec*-alkyl complex to yield the terminal olefin dihydride intermediate. The reverse process, β-hydrogen elimination of the primary alkyl to yield the internal alkyl complex, does not compete with catalytic turnover. In the absence of dihydrogen, olefin isomerization is observed and most likely proceeds through allylic C–H bond activation.[82] This reaction is also not competitive with olefin hydrogenation as no isomerized product is observed during the hydrogenolysis of either *cis*- or *trans*-2-butene.

Catalytic hydrosilation most likely proceeds through a mechanism similar to that of hydrogenation. While definitive isotopic labeling studies have not yet been performed, we believe an intermediate iron olefin complex undergoes oxidative addition of silane to yield an iron(II) olefin silyl hydride. Isolation of the iron(0) bis(silane) complex argues against direct oxidative addition to the L$_3$Fe(0) fragment. The observed products are most likely a result of ligand-induced oxidative addition followed by Chalk–Harrod or modified Chalk–Harrod insertion and reductive elimination pathways.[70,72] More detailed kinetic, isotopic labeling, and mechanistic studies are currently under investigation, and the results of these studies will be reported in due course.

Experimental Section

General Considerations. All air- and moisture-sensitive manipulations were carried out using standard vacuum line, Schlenk, and cannula techniques or in an M. Braun inert atmosphere drybox containing an atmosphere of purified nitrogen. The M. Braun drybox was equipped with a cold well designed for freezing samples in liquid nitrogen.

Solvents for air- and moisture-sensitive manipulations were initially dried and deoxygenated using literature procedures.[83] Argon and hydrogen gas were purchased from Airgas Inc. and passed through a column containing manganese oxide supported on vermiculite and 4 Å molecular sieves before admission to the high-vacuum line. Benzene-d_6 and toluene-d_8 were purchased from Cambridge Isotope Laboratories, distilled from sodium metal under an atmosphere of argon, and stored over 4 Å molecular sieves or sodium metal. 1-Hexene, cyclohexene, 1-methylcyclohexene, styrene, phenylsilane, and diphenylsilane were purchased from Acros, dried over LiAlH$_4$ and either vacuum transferred or distilled before use. Norbornene was purchased from Acros and dried over LiAlH$_4$ by melting at 60 °C in an evacuated vessel and stirring for 24 h. The olefin was separated from the drying agent by vacuum transfer. (+)-(*R*)-Limonene and α-methylstyrene were purchased from Aldrich, dried over LiAlH$_4$, and vacuum distilled. Diphenylacetylene was recrystallized from pentane, dried under high vacuum for 16 h, and then recrystallized from dry pentane in the drybox. Carbon monoxide was purchased from Aldrich and passed through a liquid nitrogen cooled trap immediately before use. The ligands (2,6-CHMe$_2$C$_6$H$_3$)$_2$N═CMe)$_2$C$_5$H$_3$N, **1-Cl$_2$**,[16] and **1-Br$_2$** were prepared according to literature procedures.

^{1}H NMR spectra were recorded on Varian Mercury 300 and Inova 400 and 500 spectrometers operating at 299.763, 399.780, and 500.62 MHz, respectively. All chemical shifts are reported relative to the peak for SiMe$_4$ using [1]H (residual) chemical shifts of the solvent as a secondary standard. For paramagnetic molecules, the ^{1}H NMR data are reported with the chemical shift followed by the peak width at half-height in hertz or multiplicity, the integration value, and, where possible, the peak assignment. ^{29}Si NMR spectra were recorded on an Inova 500 spectrometer operating at 99.320 MHz, and were referenced to that for 50% SiMe$_4$ in toluene.

Single crystals suitable for X-ray diffraction were coated with polyisobutylene oil in a drybox and were quickly transferred to the goniometer head of a Siemens SMART CCD area detector system equipped with a molybdenum X-ray tube ($\lambda = 0.71073$ Å). Preliminary data revealed the crystal system. A hemisphere routine was used for data collection and determination of lattice constants. The space group was identified, and the data were processed using the Bruker SAINT program and corrected for absorption using SADABS. The structures were solved using direct methods (SHELXS) completed by subsequent Fourier synthesis and refined by full-matrix least-squares procedures.

All calculations were performed with the Amsterdam Density Functional (ADF2003.01) suite of programs.[84–86] Relativistic effects were included using the zero-order regular approximation. The Vosko, Wilk, and Nusair (VWM) local density approximation[87] and Becke's exchange[88] and Perdew's correlation[89] (BP86) were used. The cores of the atoms were frozen up to 1s for C, N, and O and 2p for Fe. Uncontracted Slater-type orbitals (STOs) of triple-ζ quality with two polarizations were employed. This basis set is denoted TZ2P in the ADF program. Each geometry optimization was carried out without

(83) Pangborn, A. B.; Giardello, M. A.; Grubbs, R. H.; Rosen, R. K.; Timmers, F. J. *Organometallics* **1996**, *15*, 1518.
(84) te Velde, G.; Bickelahaupt, F. M.; van Gisbergen, S. J. A.; Fonseca Guerra, C.; Barends, E. J.; Snijders, J. G.; Zielger, T. *J. Comput. Chem.* **2001**, *22*, 931.
(85) Fonseca Guerra, C.; Snijders, J. G.; te Velde, G.; Baerend, E. J. *Theor. Chem. Acc.* **1998**, *99*, 391.
(86) Baerends, E. J.; Autschbach, J. A.; Berces, A.; Bo, C.; Boerrigter, P. M.; Cavallo, L.; Chong, D. P.; Deng, L.; Dickson, R. M.; Ellis, D. E.; Fan, L.; Fischer, T. H.; Guerra Fonseca, C.; van Gisbergen, S. J. A.; Groeneveld, J. A.; Gritsenko, O. V.; Grüning, M.; Harris, F. E.; van den Hoek, P.; Jacobsen, H.; van Kessel, G.; Koostra, F.; van Lenthe, E.; Osinga, V. P.; Patchkovshii, S.; Philipsen, P. H. T.; Post, D.; Pye, C. C.; Ravenek, W.; Ros, P.; Schipper, P. R. T.; Schreckenbach, G.; Snijders, J. G.; Sola, M.; Swart, M.; Swerhone, D.; te Velde, G.; Vernooijs, P.; Versluis, L.; Visser, O.; van Wezenbeek, E.; Wiesenekker, G.; Wolff, S. K.; Woo, T. K.; Ziegler, T. ADF2002.03, SCM, Theoretical Chemistry, Vrije Universiteit, Amsterdam, The Netherlands; http://www.scm.com/.
(87) Vosko, S. H.; Wilk, L.; Nusair, M. *Can. J. Phys.* **1990**, *58*, 1200.
(88) Becke, A. D. *Phys. Rev.* **1988**, *A38*, 2398.
(89) Perdew, J. P. *Phys. Rev.* **1986**, *B33*, 8822.

symmetry constraints. The orbital pictures shown in Figure 4 were generated using MOLEKEL[90] to process the ADF results.

Catalytic reactions were assayed by gas chromatography by comparison to authentic samples. Gas chromatography was performed on a Shimadzu GC-2010 gas chromatograph equipped with an RTX-5 capillary column (15 m) with an injector temperature of 250 °C and a detector temperature of 250 °C. The methods used for separating hydrogenation substrates and products are as follows: cyclohexene/cyclohexane, 1-hexene/n-hexane, 1,5-hexadiene/n-hexane, and 1-methylcyclohexene/methylcyclohexane used an oven temperature of 27 °C for 12 min, with a ramp rate of 40 °C/min to a final temperature of 150 °C for 10 min, (+)-(R)-limonene/(+)-p-menth-1-ene and norbornene/norbornane used an oven temperature of 50 °C for 30 min, and styrene/ethylbenzene, α-methylstyrene/cumene, and α-ethylstyrene/2-phenyl-1-butene used an oven temperature of 80 °C for 2 min, with a ramp rate of 10 °C/min to a final temperature of 110 °C for 20 min. The methods used for separating hydrosilation substrates and products are as follows: cyclohexene, 1-hexene, and 1,5-hexadiene from the products used an oven temperature of 80 °C for 2 min, with a ramp rate of 10 °C/min to a final temperature of 110 °C for 20 min, (+)-(R)-limonene, styrene, α-methylstyrene, and diphenylacetylene from the products used an oven temperature of 120 °C for 1 min, with a ramp rate of 20 °C/min to a final temperature of 240 °C for 15 min.

UV−vis spectra were recorded on a Hewlett-Packard 8543E spectrophotometer. Absorbance spectra were collected from 300 to 1100 nm. Stock solutions were prepared by dissolving 0.005 g of the desired compound in pentane and diluting to 25.00 mL. Subsequent solutions for Beer's law plots were made with 2.00, 3.00, or 4.00 mL of stock solution and dilution of the sample to 6.00 mL. Solution infrared spectra were recorded with an in situ IR spectrometer fitted with a 30-bounce, silicon-tipped probe optimized for sensitivity. The spectra were acquired in 16 scans (30 s intervals) at a gain of 1 and a resolution of 4. A representative reaction was carried out as follows: The IR probe was inserted through a nylon adapter and O-ring seal into a flame-dried, cylindrical flask fitted with a magnetic stir bar and T-joint. The T-joint was capped by a septum for injections and a nitrogen line. Following evacuations under full vacuum and flushing with nitrogen, the flask was charged with toluene and a background was recorded at ambient temperature and at −78 °C. The flask was then charged with a toluene solution of 1-N$_2$ to make the final reaction volume 10.0 mL with approximately 0.005 M concentration. The samples were cooled using an acetone/dry ice bath. The reactions were recorded between 20 and 40 intervals.

Preparation of (^{iPr}PDI)Fe(N$_2$)$_2$ (1-(N$_2$)$_2$): Method 1. A 100 mL round-bottomed flask was charged with 9.96 g (49.8 mmol) of mercury and approximately 15 mL of pentane. The resulting slurry was chilled to −35 °C in the drybox freezer. Sodium (0.050 g, 2.2 mmol) was cut into small pieces and added slowly to the cold mercury slurry with stirring. Once all of the sodium was added, the resulting amalgam was stirred in a N$_2$ atmosphere for 20 min to ensure complete dissolution of the metal. A pentane slurry containing 0.300 g (0.431 mmol) of 1-Br$_2$ was added to the flask containing the amalgam. The reaction was stirred vigorously, forming a dark green solution and white precipitate. After 48 h, the reaction mixture was decanted away from the amalgam, and the resulting green solution was filtered through Celite to remove the NaBr. Removing the solvent in vacuo yielded a brown solid which after recrystallization from an ether/pentane (∼1:1) mixture afforded 0.160 g (63%) of a green crystalline solid identified as 1-(N$_2$)$_2$. Anal. Calcd for C$_{33}$H$_{43}$N$_7$Fe: C, 66.77; H, 7.30; N, 16.52. Found: C, 66.49; H, 7.52; N, 16.44. IR (KBr): ν_{N_2} 2053, 2124 cm^{-1}. IR (toluene, −78 °C): ν_{N_2} = 2058, 2122 cm^{-1}. IR (pentane, 23 °C): ν_{N_2} = 2132, 2073 cm^{-1}. In solution the molecule loses 1 equiv of N$_2$ over time to afford 1-N$_2$. ^{1}H NMR (benzene-d_6, 22 °C): δ = −0.31 (d, 8 Hz, 12H,

(90) Flukiger, P.; Luthi, H. P.; Portmann, S.; Weber, J. MOLEKEL 4.3, Swiss Center for Scientific Computing, Manno, Switzerland, 2000; http://www.cscs.ch/molekel.

CHMe_2), 0.75 (sept, 16 Hz, 4H, CHMe$_2$), 1.13 (d, 8 Hz, 12H, CHMe_2), 2.58 (s, $\Delta\nu_{1/2}$ = 20 Hz, 1H, p-Pyr), 7.68 (m, 6H, m,p-aryl), 10.11 (d, 10 Hz, 2H, p-Pyr), 13.61 (s, $\Delta\nu_{1/2}$ = 56 Hz, 6H, N═C(Me)). IR (toluene, 23 °C): ν_{N_2} = 2036 cm^{-1}. IR (pentane): ν_{N_2} = 2046 cm^{-1}.

Preparation of 1-(N$_2$)$_2$: Method 2. A 50 mL round-bottomed flask was charged with 0.102 g (0.15 mmol) of 1-Br$_2$ and approximately 30 mL of diethyl ether. The resulting blue suspension was cooled to −35 °C in the drybox freezer. Via microsyringe, 0.293 mL (0.293 mmol) of a 1.0 M solution of NaBEt$_3$H in toluene was added to the reaction flask. After being stirred under a N$_2$ atmosphere at ambient temperature for 3 h, the green-purple solution was filtered through Celite, and the volatiles were removed from the filtrate in vacuo. Recrystallization of the resulting residue from pentane at −35 °C afforded analytically and spectroscopically pure 1-(N$_2$)$_2$.

Preparation of (^{iPr}PDI)Fe(CO)$_2$ (1-(CO)$_2$). A thick-walled glass vessel was charged with 0.030 g (0.051 mmol) of 1-(N$_2$)$_2$, approximately 10 mL of pentane, and a stir bar. On the high-vacuum line, 1 atm of CO was added. Upon addition, the dark green solution turned green-red. After the solution was stirred for 1 h, the excess CO and solvent were removed in vacuo to yield 0.026 g (88%) of an olive green solid identified as 1-(CO)$_2$. Anal. Calcd for C$_{35}$H$_{43}$N$_3$O$_2$Fe: C, 70.82; H, 7.30; N, 7.08. Found: C, 70.60; H, 6.94; N, 6.89. ^{1}H NMR (benzene-d_6): δ = 0.96 (d, 8 Hz, 12H, CHMe_2), 1.40 (d, 8 Hz, 12H, CHMe_2), 2.08 (s, 6H, C(Me)), 2.77 (q, 16 Hz, 4H, CHMe$_2$), 7.12−7.23 (m,p-aryl, p-Pyr), 7.63 (d, 10 Hz, 2H, m-Pyr). ^{13}C NMR (benzene-d_6): δ = 16.21 (C(Me)), 24.57 (CHMe_2), 25.00 (CHMe_2), 27.70 (CHMe$_2$), 117.525, 121.38, 123.75, 126.62, 140.30, 145.53, 149.78, 155.68 (aryl, Pyr, imine). IR(pentane): ν_{CO} = 1914, 1974 cm^{-1}.

Toepler Pump Experiment for Characterization of 1-(N$_2$)$_2$. A 100 mL round-bottomed flask was charged with 0.095 g (0.16 mmol) of 1-(N$_2$)$_2$ and 0.030 g (0.17 mmol) of diphenylacetylene. Vacuum-transferred pentane was collected in the flask at −78 °C. The resulting reaction mixture was stirred, forming a red solution and liberating dinitrogen. The free dinitrogen was collected with the aid of a Toepler pump into a volume of 71.7 mL. After approximately 2 h, 68 Torr (82%) of dinitrogen was collected. Similar experiments were conducted for the solution characterization of 1-N$_2$ and 1-H$_2$, where 86% and 82% of the expected amount of gas was collected. In the case of 1-H$_2$, the gas that was collected was burned, confirming its identity as H$_2$.

General Hydrogenation Procedure with 1-(N$_2$)$_2$. A thick-walled glass vessel was charged with 0.008 g (0.02 mmol) of 1-(N$_2$)$_2$, approximately 4 mL of toluene, and a stir bar. Approximately 4.90 mmol of substrate was added to the vessel. The vessel was submerged in liquid nitrogen and evacuated. One atmosphere of hydrogen was admitted and the reaction mixture warmed to ambient temperature and stirred for the appropriate time. The progress of the reaction was assayed periodically by gas chromatography.

General Hydrogenation Procedure with 1-(N$_2$)$_2$: Neat Olefin. A thick-walled glass vessel was charged with 0.004 g (0.008 mmol) of 1-(N$_2$)$_2$ and a stir bar. Approximately 2 mL of the alkene was added by vacuum transfer into a calibrated tube followed by a second vacuum transfer into the thick-walled glass vessel. The vessel was submerged in liquid nitrogen and evacuated. One atmosphere of dihydrogen was added to the vessel at −196 °C and the reaction warmed to ambient temperature.

General Hydrosilation Procedure. A 6 mL vial fitted with a PTFE silicon septum was charged with 0.002 g of 1-(N$_2$)$_2$, 1 mL of pentane, and a stir bar. To the resulting green solution were added 1.23 mmol of the desired olefin and silane (PhSiH$_3$ or Ph$_2$SiH$_2$). Immediately upon the addition of olefin, the solution changed color from green to red. The resulting reaction mixture was stirred for the indicated amount of time (Table 4), and periodic aliquots of the reaction mixture were quenched with water−pentane mixtures and analyzed by GC and NMR spectroscopy. The identity of each product was compared to literature

values.[91] One product, Ph(PhSiH$_2$)C=C(H)Ph, has not been previously reported and has been characterized as follows: ^{1}H NMR (benzene-d_6): δ = 4.97 (s, 2H, Si*H*), 6.8−7.14 (m, 14H, aryl and C*H*), 7.47 (d, 2H, aryl). ^{13}C NMR (benzene-d_6): δ = 127.09 (CH), 128.51 (CH), 128.35 (CH), 128.69 (CH), 128.80 (CH), 129.55 (CH), 130.37 (CH), 130.57 (CH), 131.95 (C), 136.43 (CH), 137.60 (C), 139.31 (C), 142.20 (C), 143.28 (CH).

Preparation of (^{iPr}PDI)Fe(PhC≡CPh) (1-(PhC≡CPh)). A 20 mL scintillation vial was charged with 0.046 g (0.078 mmol) of **1-(N$_2$)$_2$** dissolved in approximately 5 mL of pentane, forming a dark green solution. Diphenylacetylene (0.014 g, 0.078 mmol) was added with stirring. Immediately upon addition, a dark red solution formed which was filtered through a pad of Celite to remove any particulates. The solvent was removed in vacuo, and the resulting red solid was recrystallized from pentane at −35 °C to afford 0.050 g (91%) of **1-(PhC≡CPh)**. Anal. Calcd for C$_{47}$H$_{53}$N$_3$Fe: C, 78.86; H, 7.46; N, 5.87. Found: C, 78.35; H, 7.12; N, 5.47. Magnetic susceptibility (benzene-d_6): μ_{eff} = 2.71 μ_B. ^{1}H NMR (benzene-d_6): δ = −1.1 ($\Delta\nu_{1/2}$ = 33), −2.6 ($\Delta\nu_{1/2}$ = 370), −5.6 ($\Delta\nu_{1/2}$ = 320), −18.4 ($\Delta\nu_{1/2}$ = 970), −34.6 ($\Delta\nu_{1/2}$ = 188), −40.4 ($\Delta\nu_{1/2}$ = 106).

Preparation of (^{iPr}PDI)Fe(η^2-SiH$_3$Ph)$_2$ (1-(Si)$_2$). A 20 mL scintillation vial was charged with 0.050 g (0.084 mmol) of **1-(N$_2$)$_2$** dissolved in approximately 5 mL of pentane. With stirring, 0.018 g (0.17 mmol) of PhSiH$_3$ was added, forming a brown-purple solution. The reaction mixture was concentrated and cooled to −35 °C, forming a green solution from which a green solid was deposited. Additional material can be isolated by taking the mother liquor and repeating the above procedure. Anal. Calcd for C$_{45}$H$_{59}$N$_3$FeSi$_2$: C, 71.68; H, 7.89; N, 5.57. Found: C, 71.51; H, 8.17; N, 5.49. Magnetic susceptibility (benzene-d_6): μ_{eff} = 2.68 μ_B. ^{1}H NMR (benzene-d_6, 23 °C): δ = −6.69 (s, 1H, η^2-SiH (basal)), −0.04 (5.5 Hz, 12H, CH*Me$_2$*), 0.92−1.09 (40.46, CH*Me$_2$* and others), 1.851 (30.52, 3H), 2.82 (34.17, 4H), 3.44 (18.55, 1H, *p*-Pyr), 3.97 (6.38, 6H), 7.04−7.18 (m, includes toluene-d_8), 7.39 (13.82, 2H), 7.57 (2.10, 4H), 7.87 (25.28, 1H), 8.39 (19.86, 1H), 9.70 (3.52, 2H), 11.46 (32.23, 6H, C(*Me*)). ^{1}H NMR (toluene-d_8, −40 °C): δ = −6.80 (s, 1H, η^2-SiH (basal)), 0.05 (s, 1H, η^2-SiH (apical)), 0.67 (d, 6.5 Hz, 6H, CH*Me$_2$*), 0.75 (d, 6.5 Hz, 6H, CH*Me$_2$*), 0.81 (d, 6.5 Hz, 6H, CH*Me$_2$*), 0.95 (d, 6.5 Hz, 6H, CH*Me$_2$*), 1.17 (d, 6 Hz, 9H), 1.84 (s, 6H, *Me*C=N), 1.90 (s, 6H), 2.55 (br s, 2H, C*H*Me$_2$), 2.78 (s, 2H, Si*H$_2$* (apical)), 3.11 (q, 6.5 Hz, 2H, C*H*Me$_2$), 6.11 (s, 2H, Si*H$_2$* (basal)), 6.51 (d, 7 Hz, 2H, *o*-phenyl (basal)), 6.92 (d, 7.5 Hz, 2H, *m*-phenyl (basal)), 6.99 (s, 2H, *p*-Pyr, *p*-phenyl, or *m,p*-aryl), 7.00−7.22 (m, includes toluene-d_8, *p*-Pyr, *p*-phenyl, or *m,p*-aryl), 7.23 (t, 7.5 Hz, *p*-Pyr, *p*-phenyl, or *m,p*-aryl), 7.30 (t, 7 Hz, *p*-Pyr, *p*-phenyl, or *m,p*-aryl), 7.41 (d, 6.5 Hz, 2H, *m*-phenyl (apical)), 7.75 (d, 7.5 Hz, 2H, *m*-Pyr), 8.15 (d, 7 Hz, 2H, *o*-phenyl (apical)). ^{29}Si (toluene-d_8, −80 °C): δ = 50.23, −44.58 ppm.

Preparation of (^{iPr}PDI)Fe(η^2-H$_2$) (1-H$_2$). A 25 mL round-bottomed flask was charged with 0.073 g (0.123 mmol) of **1-(N$_2$)$_2$**, and the green solid was dissolved in approximately 10 mL of pentane. The flask was fitted with a 180° needle valve and attached to a high-vacuum line. After removal of the nitrogen from the drybox atmosphere by evacuation at −78 °C, the solution was warmed to ambient temperature and 1 atm of H$_2$ admitted. The resulting reaction mixture was stirred for several hours and the solvent removed in vacuo, leaving a nitrogen-sensitive brown solid identified as **1-H$_2$**. Anal. Calcd for C$_{33}$H$_{45}$N$_3$Fe: C, 73.30; H, 8.45; N, 7.83. Found: C, 73.46; H, 8.98; N, 7.60. Magnetic susceptibility (benzene-d_6): μ_{eff} = 2.70 μ_B. ^{1}H NMR (benzene-d_6): δ = −0.50 (d, 8 Hz, 12H, CH*Me$_2$*), 0.54 (q, 8 Hz, 4H, C*H*Me$_2$), 1.14 (d, 8 Hz, 12H, CH*Me$_2$*), 1.97 (t, 7.5 Hz, 1H, *p*-Pyr), 7.74 (m, 6H, *m,p*-aryl), 10.40 (d, 9 Hz, 2H, *m*-Pyr), 15.09 (20.78, 6H, C(*Me*)).

Conclusions

Synthesis and characterization of an unusual high spin, square pyramidal iron(0) bis(dinitrogen) complex supported by a pyridinediimine ligand have been accomplished. In solution, this molecule loses 1 equiv of N$_2$ to form a four-coordinate iron(0) dinitrogen complex. Both N$_2$ complexes allow access to the rich chemistry of the L$_3$Fe(0) fragment under mild, thermal conditions. These molecules also serve as precursors for iron(0) dihydrogen, bis(silane), and alkyne complexes. The silane and dihydrogen σ-complexes are geometrically and electronically similar to the dinitrogen complexes, while the alkyne adduct is distorted toward a pseudotetrahedral geometry. All of these molecules serve as effective precatalysts for the hydrogenation and hydrosilation of olefins and alkynes under mild conditions. The catalytic reactions proceed with levels of activity and selectivity that rival those of traditional precious metal catalysts. Isotopic labeling studies established that terminal olefins such as 1-butene and 1-hexene do not undergo alkyl isomerization competitive with the catalytic reactions, although olefin isomerization is observed in the absence of H$_2$ or silane. Overall, this study has demonstrated that iron, when in the appropriate coordination geometry and spin state, is a reasonable alternative to toxic, precious metals in designing catalytic processes.

Supporting Information Available: Additional NMR, computational, UV−vis, and magnetic data and experimental details for **2-Cl$_3$** (PDF) and crystallographic data for **1-(N$_2$)$_2$**, **1-(Ph-C≡CPh)**, **1-(Si)$_2$**, and **2-Cl$_3$** including full atom-labeling schemes and bond distances and angles (CIF). This material is available free of charge via the Internet at http://pubs.acs.org.

JA046753T

(91) (a) Fu, P.-F.; Brard, L.; Li, Y.; Marks, T. J. *J. Am. Chem. Soc.* **1995**, *117*, 7157. (b) Molander, G. A.; Julius, M. *J. Org. Chem.* **1992**, *57*, 6347. (c) Glaser, P. B.; Tilley, T. D. *J. Am. Chem. Soc.* **2003**, *125*, 13640.